Langmuir Turbulence Parameterization in Tropical Cyclone Conditions

BRANDON G. REICHL

Graduate School of Oceanography, University of Rhode Island, Narragansett, Rhode Island

DONG WANG

College of Earth, Ocean, and Environment, University of Delaware, Newark, Delaware

TETSU HARA AND ISAAC GINIS

Graduate School of Oceanography, University of Rhode Island, Narragansett, Rhode Island

TOBIAS KUKULKA

College of Earth, Ocean, and Environment, University of Delaware, Newark, Delaware

ABSTRACT

The Stokes drift of surface waves significantly modifies the upper-ocean turbulence because of the Craik–Leibovich vortex force (Langmuir turbulence). Under tropical cyclones the contribution of the surface waves varies significantly depending on complex wind and wave conditions. Therefore, turbulence closure models used in ocean models need to explicitly include the sea state–dependent impacts of the Langmuir turbulence. In this study, the K-profile parameterization (KPP) first-moment turbulence closure model is modified to include the explicit Langmuir turbulence effect, and its performance is tested against equivalent large-eddy simulation (LES) experiments under tropical cyclone conditions. First, the KPP model is retuned to reproduce LES results without Langmuir turbulence to eliminate implicit Langmuir turbulence effects included in the standard KPP model. Next, the Lagrangian currents are used in place of the Eulerian currents in the KPP equations that calculate the bulk Richardson number and the vertical turbulent momentum flux. Finally, an enhancement to the turbulent mixing is introduced as a function of the nondimensional turbulent Langmuir number. The retuned KPP, with the Lagrangian currents replacing the Eulerian currents and the turbulent mixing enhanced, significantly improves prediction of upper-ocean temperature and currents compared to the standard (unmodified) KPP model under tropical cyclones and shows improvements over the standard KPP at constant moderate winds ($10 \, \mathrm{m \, s^{-1}}$).

1. Introduction

Tropical cyclone prediction models require sea surface temperature and currents to accurately compute air–sea heat and momentum fluxes. These air–sea fluxes are the primary contributors to the energy budget of a tropical cyclone and therefore greatly affect the storm intensity (see Emanuel 1991, 1999). Tropical cyclones are known to generate vigorous responses in the upper ocean, which include surface waves with amplitudes larger than 15 m,

upper-ocean currents in excess of $1 \, \mathrm{m \, s^{-1}}$, and sea surface temperature cooling of several degrees (Ginis 2002). The surface temperature and current responses to wind forcing are determined by turbulent mixing throughout the upper-ocean boundary layer, which must be carefully accounted for in ocean models that are coupled to tropical cyclone forecast models.

As a hurricane passes over a particular location, the upper-ocean mixing develops in the following manner: First, near-surface ocean currents and surface waves increase as momentum from the wind is transferred into the ocean. The large vertical shear below the developing surface current generates turbulence and drives the deepening of the active surface mixing layer. Surface gravity waves also contribute to the upper-ocean mixing

Corresponding author address: B. G. Reichl, Graduate School of Oceanography, University of Rhode Island, 215 S. Ferry Rd., Narragansett, RI 02882.
E-mail: breichl@my.uri.edu

and the turbulent kinetic energy (TKE) budget through breaking and the Stokes drift; the latter significantly modifies upper-ocean turbulence (Langmuir turbulence). The near-surface temperature cools due to the entrainment of cold water from the thermocline below as the mixing layer deepens (Price 1981). Although these are primarily one-dimensional (vertical) mixing processes, the cool-water entrainment under a tropical cyclone can be further enhanced by three-dimensional processes, notably by upwelling due to Ekman pumping (Yablonsky and Ginis 2009). Evaporation is another source of surface cooling, although this is generally a second-order process during strong winds and active entrainment (Ginis 2002).

In three-dimensional ocean circulation models that utilize Reynolds-averaged equations of motion, the upper-ocean turbulent fluxes are typically parameterized by closure models. The traditional turbulence closure models (e.g., Mellor and Yamada 1982; Large et al. 1994) determine the evolution of the mixing layer turbulence through inputs including the wind stress τ (or the friction velocity $u_* = \sqrt{\tau/\rho_a}$, where ρ_a is the air density) and the surface buoyancy flux B_*. These closure models do not explicitly capture the contribution of surface gravity waves to the upper-ocean turbulence. One source of upper-ocean turbulence due to surface gravity waves is the injection of TKE from wave breaking to the ocean (Melville 1996). The elevated turbulence due to breaking waves decays within depths scaling with the significant wave height (i.e., Craig and Banner 1994; Terray et al. 1996). Another significant source of turbulence derived from surface waves is the Langmuir turbulence. The depth scale of the Langmuir turbulence is typically larger and is determined by the mixed layer depth and/or the Stokes drift e-folding depth (Harcourt and D'Asaro 2008; Grant and Belcher 2009; Sullivan et al. 2012).

First observed by Langmuir (Langmuir 1938), it took several decades for the mechanism that drives Langmuir circulations to be identified. This is the Craik–Leibovich (CL) vortex force, which results from interaction between the Stokes drift of surface waves and the upper-ocean Eulerian current vorticity (Craik and Leibovich 1976). In the high Reynolds number planetary boundary layer turbulence, the Langmuir turbulence (turbulence that is modified by the CL vortex force) exists over scales ranging from $O(1)$ m to the mixed layer depth, even when not organized as coherent Langmuir circulations (McWilliams et al. 1997). Langmuir turbulence has been extensively studied for the last two decades using large-eddy simulation (LES) models that can resolve explicitly the dominant scales of Langmuir turbulence (Skyllingstad and Denbo 1995; McWilliams et al. 1997; Skyllingstad et al. 2000; Noh et al. 2004; Min

and Noh 2004; Polton and Belcher 2007; Sullivan et al. 2007; Harcourt and D'Asaro 2008; Grant and Belcher 2009; Kukulka et al. 2009; Teixeira and Belcher 2010; Kukulka et al. 2010; Noh et al. 2011; Van Roekel et al. 2012). All support the conclusion that the CL vortex force strengthens upper-ocean mixing in many different regimes. Studies that qualitatively and quantitatively compare LES results to in situ data confirm that including the CL vortex force improves the model observation agreement (Kukulka et al. 2009; D'Asaro et al. 2014).

LES has also been used to study stochastic momentum injection via wave breaking in the presence of Langmuir turbulence in the planetary boundary layer (Noh et al. 2004; Sullivan et al. 2007; McWilliams et al. 2012). These studies show that the impact of intermittent breaking momentum injection is mostly limited to the upper several meters when compared to constant surface momentum fluxes. Therefore, the CL vortex force (which impacts scales of 10–200 m) is a much more effective mechanism to enhance mixed layer deepening. Various scalings for the enhancement of the turbulence closure models based on the Langmuir number have been proposed, which will be discussed in detail later (sections 2 and 8).

Sullivan et al. (2012) have employed LES to study Langmuir turbulence under strong, transient wind stress and Stokes drift conditions characteristic of tropical cyclones. This idealized study shows large variation in Langmuir turbulence from the right to the left side of the storm track. The right side of the storm (Northern Hemisphere convention) has inertially resonant wind and current rotation, which significantly deepens the mixing layer compared to the nonresonant left side (Price 1981; Skyllingstad et al. 2000; Sanford et al. 2011). The right side also has larger waves due to resonance between the wind and the storm translation (Young 2003; Moon et al. 2003), which results in a stronger, deeper Stokes drift profile (Sullivan et al. 2012).

Recently, Rabe et al. (2015) investigated Langmuir turbulence under Hurricane Gustav (2008) by combining in situ measurements of turbulence obtained by Lagrangian floats deployed ahead of the storm and LES hindcasts of the upper-ocean turbulence at the float locations. The observations show a regime behind the eye of a tropical cyclone where the turbulent vertical velocity variance $\overline{w'^2}$ is reduced compared to traditional wind-driven u_* scaling. The LES results suggest that such a regime may be due to large variability of the Langmuir turbulence, since the local wave field varies significantly (both in time and in space) under a tropical cyclone. Comparisons between the turbulent quantities from the LES and the observations are imperfect for

various reasons, particularly because of uncertainty of the drag coefficient in tropical cyclone conditions (see Rabe et al. 2015). Nevertheless, the results suggest that the Langmuir turbulence is an important, spatially variable source of mixing under a tropical cyclone and that the additional mixing due to the CL vortex force is necessary to best match the simulations and the field observations.

To improve the comparison between models containing the Langmuir turbulence and in situ data, large-scale three-dimensional processes such as upwelling and advection must be included. However, such models are computationally expensive and cannot be run at resolutions that are needed to resolve the dominant Langmuir turbulence scale. Therefore, turbulence closure models that parameterize Langmuir turbulence must be developed and be included in coarse-resolution $[O(10^3–10^4)\,\mathrm{m}]$ basin-scale numerical ocean models. Such an approach would contribute to improved performance of coupled hurricane–wave–ocean simulation/prediction models.

The main objective of this study is to develop a robust turbulence closure model that accurately accounts for the Langmuir turbulence effects under tropical cyclone conditions. Such a model is constructed and tested using an extensive set of LES Langmuir turbulence experiments under a wide range of tropical cyclone wind and wave conditions.

2. Geophysical turbulence closure models

In typical ocean models based on Reynolds-averaged Navier–Stokes (RANS) equations, the horizontal momentum equations, with the hydrostatic and Boussinesq approximations, can be expressed as

$$\frac{\partial \mathbf{U}_h}{\partial t} + \left(\mathbf{U}_h \cdot \frac{\partial}{\partial \mathbf{x}_h} + W\frac{\partial}{\partial z}\right)\mathbf{U}_h + \mathbf{f} \times \mathbf{U}_h$$
$$= -\frac{1}{\rho_0}\frac{\partial P}{\partial \mathbf{x}_h} - \frac{\partial}{\partial z}\left(\nu\frac{\partial \mathbf{U}_h}{\partial z} + \overline{\mathbf{u}_h' w'}\right), \qquad (1)$$

where $\mathbf{x}_h$ are the horizontal coordinates, z is the vertical coordinate (positive upward), $\mathbf{f}$ is the Coriolis parameter (vector), ν is the molecular viscosity, and ρ_0 is the reference density. The instantaneous horizontal velocity vector $\mathbf{u}_h$ and vertical velocity w are decomposed into the Reynolds mean ($\mathbf{U}_h$, W) and fluctuation ($\mathbf{u}_h'$, w'), and P is the Reynolds-averaged dynamic pressure. The overbar represents the Reynolds mean, and $\overline{\mathbf{u}_h' w'}$ is the vertical turbulent momentum flux. The horizontal turbulent fluxes have been neglected. The temperature advective–diffusive equation can be expressed as

$$\frac{\partial \Theta}{\partial t} + \mathbf{U}_h \cdot \frac{\partial \Theta}{\partial \mathbf{x}_h} + W\frac{\partial \Theta}{\partial z} = -\frac{\partial}{\partial z}\left(\nu_\theta\frac{\partial \Theta}{\partial z} + \overline{\theta' w'}\right), \qquad (2)$$

where the potential temperature θ is similarly decomposed into the Reynolds mean Θ and fluctuation θ', and ν_θ is the molecular diffusion of heat. Again, horizontal turbulent fluxes have been dropped.

In the presence of the wave-induced Stokes drift profile $\mathbf{u}_S$, the advective and planetary terms in the momentum equation contain the Stokes drift (following McWilliams and Restrepo 1999):

$$\frac{\partial \mathbf{U}_h}{\partial t} + \left(\mathbf{U}_h \cdot \frac{\partial}{\partial \mathbf{x}_h} + W\frac{\partial}{\partial z}\right)\mathbf{U}_h + \mathbf{f} \times (\mathbf{U}_h + \mathbf{u}_S)$$
$$+ \boldsymbol{\omega} \times \mathbf{u}_S = -\frac{1}{\rho_0}\frac{\partial \tilde{P}}{\partial \mathbf{x}} - \frac{\partial}{\partial z}\left(\nu\frac{\partial \mathbf{U}_h}{\partial z} + \overline{\mathbf{u}_h' w'}\right), \qquad (3)$$

where $\boldsymbol{\omega} = \nabla \times \mathbf{U}_h$ is the vertical (relative) vorticity vector, the advective Stokes drift component is represented through the vortex force $\boldsymbol{\omega} \times \mathbf{u}_S$, the planetary rotation term is modified to include the Stokes drift (the Coriolis–Stokes term), and the dynamic pressure $\tilde{P}$ has been modified to include the Stokes drift correction. Similarly, the Stokes drift is introduced to the advective terms of the temperature equation

$$\frac{\partial \Theta}{\partial t} + (\mathbf{U}_h + \mathbf{u}_S) \cdot \frac{\partial \Theta}{\partial \mathbf{x}_h} + W\frac{\partial \Theta}{\partial z} = -\frac{\partial}{\partial z}\left(\nu_\theta\frac{\partial \Theta}{\partial z} + \overline{\theta' w'}\right). \qquad (4)$$

The Stokes drift should be calculated from the full wave spectra, which are prescribed based on observations or surface wave models. Therefore, the only components of the system that cannot be solved for by the horizontal momentum equation [(3)], the temperature–advection equation [(4)], the equation of state, and the continuity equation are the vertical turbulent flux terms. A turbulence closure model is used to calculate these terms, which can be expressed as

$$\overline{\mathbf{u}_h' w'} = -K_M\frac{\partial \mathbf{U}_h}{\partial z} + \Gamma_U, \quad \text{and} \qquad (5)$$

$$\overline{\theta' w'} = -K_\theta\frac{\partial \Theta}{\partial z} + \Gamma_\theta, \qquad (6)$$

where the vertical turbulent flux of a property is equal to the vertical gradient of the mean property multiplied by an eddy viscosity K_M (or an eddy diffusivity K_θ for temperature) plus a nonlocal (or countergradient) term Γ. The K-profile parameterization (KPP; Large et al. 1994) is one example of a turbulent closure model for geophysical applications that solves for the turbulent fluxes following this form. Recently, several studies

(McWilliams and Sullivan 2000; Smyth et al. 2002; McWilliams et al. 2012, 2014; Sinha et al. 2015) proposed modifications to the KPP model that include the Langmuir turbulence.

In McWilliams and Sullivan (2000), the Langmuir turbulence is included via an enhancement factor to the eddy viscosity (and diffusivity) through an enhanced turbulent velocity scale. The enhancement factor is parameterized from the turbulent Langmuir number:

$$\mathrm{La}_t = \sqrt{\frac{u_*}{|\mathbf{u}_S(z=0)|}}, \qquad (7)$$

where $|\mathbf{u}_S(z=0)|$ is the magnitude of the surface Stokes drift. This approach was later modified by Smyth et al. (2002) to include dependency on the surface buoyancy flux. Fan and Griffies (2014) showed that using this enhanced turbulent velocity scale in the MOM global ocean circulation model had significant impacts on the evolution of the temperature and mixed layer depth in certain regions. However, the enhanced velocity scale did not properly resolve model differences against in situ observations, suggesting the need for additional model improvements.

McWilliams et al. (2012) proposed further modifications to the KPP model that include an additional component of the turbulent momentum flux down the gradient of the Stokes drift:

$$\overline{\mathbf{u}'_h w'} = -K_L \frac{\partial \mathbf{U}_{hL}}{\partial z}, \qquad (8)$$

where K_L is the Lagrangian eddy viscosity, and $\mathbf{U}_{hL}$ is the Lagrangian current ($\mathbf{U}_{hL} = \mathbf{u}_S + \mathbf{U}_h$). This approach was demonstrated to improve simulations of the mean current profiles in idealized, unstratified conditions when compared to LES. McWilliams et al. (2014) suggest that for more accurate prediction of the mixing depth the KPP model may also require enhancement of the turbulent velocity scale to compute the unresolved contributions to the bulk mixed layer shear.

Other studies investigated second-moment turbulence closure models by including the CL vortex force in the TKE equation (D'Alessio et al. 1998), the dissipation length scale (Kantha and Clayson 2004), and the stability functions (Harcourt 2013, 2015). The additional turbulent flux down the gradient of the Stokes drift is a key component to the modifications presented by Harcourt (2013, 2015). These studies demonstrate that prediction of the upper-ocean current is improved if the Langmuir turbulence parameterization via Stokes drift is included in the closure model.

In this study we focus on the KPP turbulence closure model under tropical cyclone conditions. First, the performance of the standard KPP model without explicit Langmuir turbulence effects is investigated under tropical cyclone conditions. Next, we investigate how different modifications to the KPP model that include Langmuir turbulence improve the comparison with equivalent LES simulations.

3. Experimental design

Although any model performance should be validated against observations in principle, it is difficult to test the KPP model using in situ data in tropical cyclone conditions. Reliable observational data are extremely rare in high-wind environments. Furthermore, to test the KPP model it is preferable to utilize one-dimensional experiments (where horizontal variations are neglected) in order to isolate the vertical turbulent mixing from large-scale three-dimensional processes that introduce additional complications. In situ observations are inherently three-dimensional and lack the temporal and spatial distributions needed to properly test the KPP model over a robust range of conditions. Instead, we will validate the KPP model against idealized computational experiments using a LES model that explicitly resolves the Langmuir turbulence. The performance of the KPP model embedded in a one-dimensional RANS model is tested against the one-dimensional solutions derived by horizontally averaging the LES results.

The ocean surface waves are simulated using the WAVEWATCH III (WW3; Tolman 2009) surface wave model. The WW3 (v3.14) model is used with a modification to the wind input source function that has been demonstrated to well predict the peak wave spectrum under tropical cyclone conditions (Fan et al. 2009). The computational domain has a uniform deepwater (4000 m) bathymetry. The horizontal dimensions are 1800 km in the direction perpendicular to the storm translation and 3000 km in the direction of storm translation, which are large enough that the boundaries are not dynamically important to the study location. The horizontal resolution of the wave model is 8.33 km, and the wave spectrum is defined over 40 logarithmically spaced frequencies (with a minimum frequency of 0.0285 Hz) and 48 evenly spaced directions. Surface forcing is applied using a defined, idealized tropical cyclone wind stress. The wind field is constructed following the model of Holland (1980) with a realistic wind inflow angle model following Zhang and Uhlhorn (2012). The radius of maximum wind (RMW) is set as 50 km, and the maximum wind speed is set at $65\,\mathrm{m\,s}^{-1}$. The wave field is initially at rest.
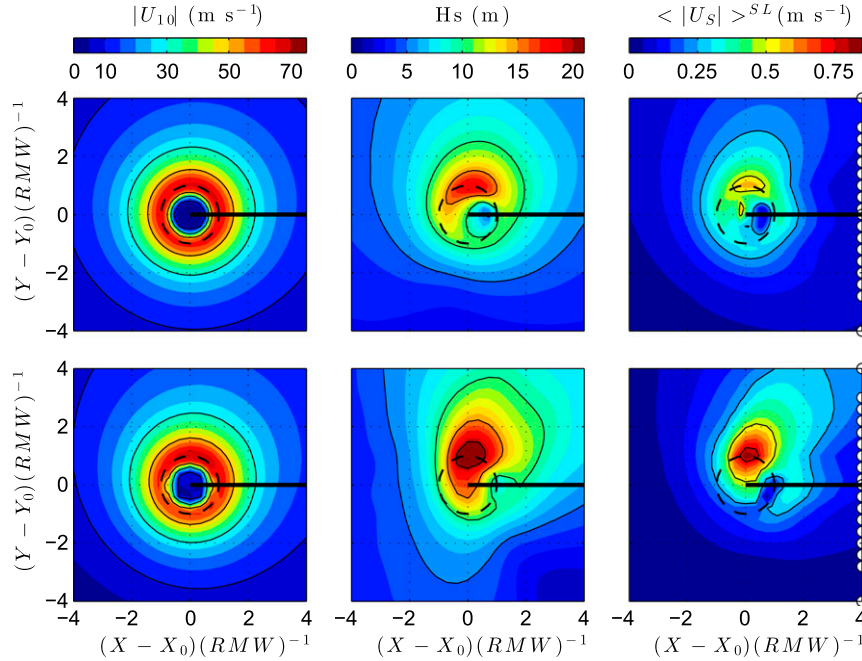
FIG. 1. (left) Wind speed, (center) significant wave height, and (right) magnitude of surface layer–averaged Stokes drift for a (top) 5 and (bottom) $10 \, \mathrm{m \, s^{-1}}$ translating idealized tropical cyclone. The horizontal and vertical axes indicate the distance from the storm center position normalized by the RMW (50 km). The white open circles in the right panels show the test site locations. The dashed circle represents RMW, and the solid black line represents the storm track (moving from right to left).

The identical wind stress is applied in the LES and one-dimensional RANS models, which are calculated using the bulk formula with the drag coefficient formulation as Sullivan et al. (2012):

$$C_d = \begin{cases} 0.0012, & : |u_{10}| < 11 \, \mathrm{m \, s^{-1}} \\ (0.49 + 0.065|u_{10}|) \times 10^{-3}, & : 11 \, \mathrm{m \, s^{-1}} \le |u_{10}| \le 20 \, \mathrm{m \, s^{-1}}, \\ 0.0018, & : 20 \, \mathrm{m \, s^{-1}} < |u_{10}| \end{cases} \tag{9}$$

where $|u_{10}|$ is the neutral 10-m wind magnitude. A very weak ($5 \, \mathrm{W \, m^{-2}}$) destabilizing surface buoyancy flux is also applied, which is insignificant after the initial onset of turbulence. Even a realistic surface heat flux does not significantly contribute to the turbulent mixing within the peak region of a tropical cyclone (wind speeds greater than $\sim 15 \, \mathrm{m \, s^{-1}}$). We therefore neglect this contribution.

The idealized tropical cyclone is translated at a constant velocity through the domain at a moderate ($5 \, \mathrm{m \, s^{-1}}$) and fast ($10 \, \mathrm{m \, s^{-1}}$) speeds. Half the translation speed vector is added to the wind speed vector to create a more realistic, asymmetric wind distribution. The resulting wind fields are shown in Fig. 1 (left panels).

The waves are spun up to a quasi-steady state (relative to the moving storm) through an initial 24-h simulation with the storm translating through the domain. The resulting significant wave height (the integrated variance spectrum) is presented in Fig. 1 (center panels) for both translation speeds. The Stokes drift is computed from the spectrum as follows:

$$\mathbf{u}_S = \int_0^{k_{UL}} \int_0^{2\pi} \Psi(k, \theta) 2\omega \exp(2kz) \mathbf{k} \, d\theta \, dk, \tag{10}$$

where $\Psi(k, \theta)$ is the wavenumber direction sea surface displacement variance spectrum, k is the wavenumber, θ is the wave direction, $\mathbf{k}$ is the wavenumber vector, $\omega = \sqrt{gk}$ is the (deep water) wave angular frequency, and k_{UL} is the upper bound of the wavenumber integration corresponding to a wavelength of 1 m. The magnitude of the Stokes drift (averaged over 20% of the mixing layer depth given by the KPP model) is shown in Fig. 1 (right panels).

TABLE 1. Location of 20 test sites for one-dimensional and LES models.

Site number	1[a]	2[a]	3[a]	4[a]	5[a]	6[a]	7[a]	8[a,b]	9[a,b]	10[a,b]
Location (km)	300	200	150	130	110	90	70	50	30	10
Site number	11[a,b]	12[a,b]	13[a,b]	14[a,b]	15[a,b]	16[a,b]	17[a,b]	18[a]	19[a,b]	20[a]
Location (km)	0	−20	−40	−60	−80	−100	−120	−140	−200	−300

[a] 10-m mixed layer.
[b] 32-m mixed layer.

The 20 test locations perpendicular to the translation direction are selected. They are given in Table 1 and plotted for reference in Fig. 1 as white circles in the right panels. At each location the time series of the wind stress and waves are used to force the LES and one-dimensional RANS models. An additional test is conducted to assess the performance of the model in lower wind conditions. A constant $10\,\mathrm{m\,s}^{-1}$ wind is applied over the entire domain. The fully developed (steady state) wave spectrum at a fetch of 2000 km is used to calculate a Stokes drift profile. The LES and one-dimensional models then calculate the turbulence and mean ocean properties for 24 h with this Stokes drift input, which is held constant. This ensures that waves are neither time or fetch limited for the constant wind experiments.

For the tropical cyclone experiments, one-dimensional and LES simulations are performed for 48 h, with the wind maximum occurring at 36 h. Comparison between the two models is performed for a duration of 24 h at each location, from 12 h before the wind maximum to 12 h after the wind maximum. This restricts the comparison between the one-dimensional simulation and the LES model to periods with higher wind. The initial potential temperature profile has a homogenous mixed layer of $\theta = 29.25°\mathrm{C}$ and a constant stratification in the interior of $-0.04\,°\mathrm{C\,m}^{-1}$, which are identical to Sullivan et al. (2012). Two initial mixed layer depths are investigated, a shallower depth of 10 m and a deeper depth of 32 m. The simulations are performed across all 20 test locations for the 10-m depth and at 11 stations for the 32-m depth. The 32-m mixed layer depth is chosen to correspond to the Sullivan et al. (2012) experiment, while the 10-m mixed layer depth is chosen as a reasonable upper limit for a shallow, summer mixed layer. For the constant wind simulation the initial mixed layer depth is 10 m, but the stratification is reduced to $-0.01°\mathrm{C\,m}^{-1}$.

The LES and one-dimensional RANS model are run with identical forcing, physical parameters, and the linear equations of state, which is defined as

$$\rho = \rho_0 + \alpha(\theta - \theta_0), \qquad (11)$$

where the reference density ρ_0 is $1026.95\,\mathrm{kg\,m}^{-3}$ for $\theta_0 = 10°\mathrm{C}$ and the salinity $S = 35\,\mathrm{psu}$. The salinity is kept constant and the thermal expansion coefficient is $\alpha = -0.2\,\mathrm{kg\,m}^{-3}\,(°\mathrm{C})^{-1}$. For the one-dimensional model, the General Ocean Turbulence Model (GOTM; Umlauf et al. 2005) is used, which includes the Coriolis–Stokes force and a modified KPP routine to account for the Langmuir turbulence.

The LES domain for the tropical cyclone experiments is $(x, y, \text{and } z) = (750, 750, \text{and } 240\,\mathrm{m})$ with a resolution of $(dx, dy, \text{and } dz) = (2.92, 2.92, \text{and } 1\,\mathrm{m})$. For the constant wind experiment, a smaller domain is used with $(x, y, \text{and } z) = (300, 300, \text{and } 180\,\mathrm{m})$ and a resolution of $(dx, dy, \text{and } dz) = (1.56, 1.56, \text{and } 0.7\,\mathrm{m})$. Our previous sensitivity tests indicated that a higher resolution or a larger domain size does not substantially change our results, indicating that our resolution is adequate. We also assessed the TKE partitioning between resolved and subgrid scale (SGS). The resolved TKE is usually greater than 75% of the total (resolved + SGS) TKE, which also supports that our resolution is sufficient. The LES model solves the SGS-averaged equations of momentum, density, and continuity following previous LES Langmuir turbulence studies (McWilliams et al. 1997). The phase-averaged momentum equations are solved in the three-dimensional coordinate system:

$$\frac{D\mathbf{u}}{Dt} + f\hat{\mathbf{z}} \times (\mathbf{u} + \mathbf{u}_S)$$
$$= -\nabla \pi - g\hat{\mathbf{z}}\left(\frac{\rho}{\rho_0}\right) + \mathbf{u}_S \times (\nabla \times \mathbf{u}) + \mathrm{SGS}, \qquad (12)$$

where the model variables are SGS averaged, $D/Dt = \partial/\partial t + \mathbf{u} \cdot \partial/\partial \mathbf{x}$, $\mathbf{x}$ is the coordinate vector, $\mathbf{u}$ is the velocity vector, $\mathbf{u}_S$ is the Stokes drift vector (the vertical component is set to 0), f is the Coriolis parameter, π is the generalized pressure $[p/\rho + 0.5(|\mathbf{u} + \mathbf{u}_S|^2 - |\mathbf{u}|^2)]$, p is the pressure, and SGS are the subgrid-scale terms described in detail by Rabe et al. (2015). Scalar (temperature) distribution is solved by the advective–diffusive equation:

$$\frac{D\rho}{Dt} + \mathbf{u}_S \cdot \nabla \rho = \mathrm{SGS}, \qquad (13)$$

where ρ is the density [determined entirely by the temperature via Eq. (11)]. Volume conservation is ensured via the incompressible continuity equation:
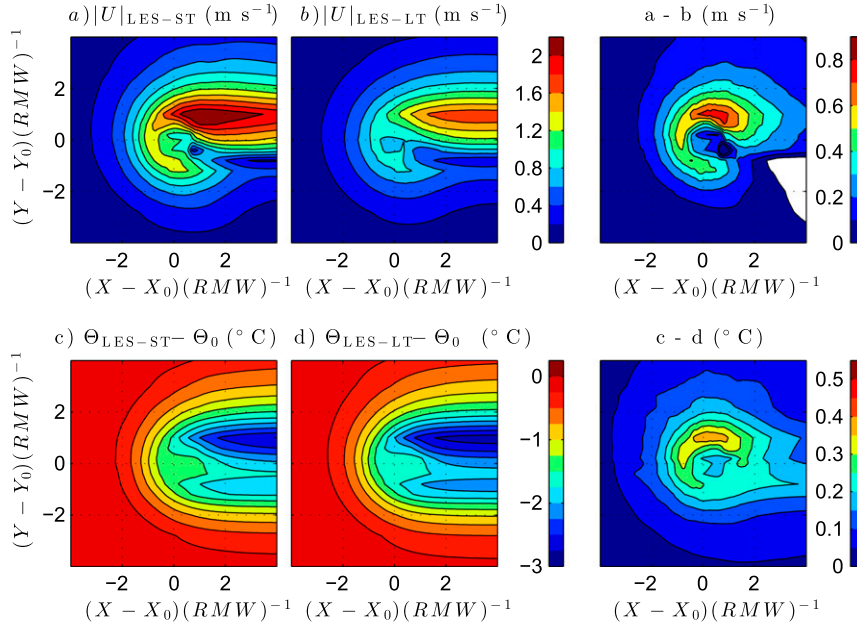
FIG. 2. (top) LES results of near-surface (at 5-m depth) current magnitude and (bottom) temperature anomaly (temperature minus initial temperature) for a $5\,\mathrm{m\,s^{-1}}$ translating tropical cyclone. The results are shown for (left) LES–ST, (center) LES–LT, and (right) the difference between the two. Note the white regions in the upper-right panel have small negative values. The horizontal and vertical axes indicate the distance from the storm center position normalized by the RMW (50 km).

$$\nabla \cdot \mathbf{u} = 0. \qquad (14)$$

The Stokes drift is included in the momentum equation via the Stokes–Coriolis force [term two on the LHS of Eq. (12)], the CL vortex force [term three on the RHS of Eq. (12)], and the generalized pressure. The Stokes drift also contributes to the temperature equation via the additional Stokes drift advection term. In general, the Langmuir turbulence has a much greater impact on the mean current profile than the Stokes–Coriolis force.

The LES is initialized in a similar manner as that described by Rabe et al. (2015). In each case, the stationary simulation is run with the initial wind, wave, and density profile until statistically stationary turbulence is achieved (e.g., for multiple eddy turnover times; h/u_*). The resulting field is then used as the initial condition for the transient LES simulation. Unlike Rabe et al. (2015), however, the mean current in the stationary solution is removed from the initial condition, such that the initial mean current is zero in both the LES and the one-dimensional model.

The LES model is first run at each test location with the Stokes drift set to zero. This means that both the Langmuir turbulence and the Coriolis–Stokes force are not simulated and the turbulence is primarily driven by vertical current shear. The results from these simulations are referred to as LES–shear turbulence (ST).

Next, the LES model is run at each location with the Stokes drift computed from the WW3 wave variance spectrum. The Stokes drift profile is calculated directly from the spectrum on the LES model vertical grid levels and linearly interpolated from the WW3 to the LES model time step. The results of these simulations will be referred to as LES–Langmuir turbulence (LT). The LES results are averaged horizontally into vertical profiles for comparing with results in the one-dimensional model.

4. LES results

In Fig. 2, we present the difference between the mean near-surface fields (temperature and currents at 5-m depth) in LES–LT and LES–ST for the tropical cyclone with $5\,\mathrm{m\,s^{-1}}$ translation speed and the 10-m initial mixed layer depth. The results with the larger translation speed and/or the deeper initial mixed layer depth are qualitatively similar. Although the actual simulations are conducted over time at fixed locations, we use the time and translation speed of the storm to transform from the temporal coordinate to the spatial coordinate (in the direction of the storm translation) to simplify the presentation. This transformation is possible because all results are presented after the wave field has reached a quasi-steady state with respect to the frame of reference
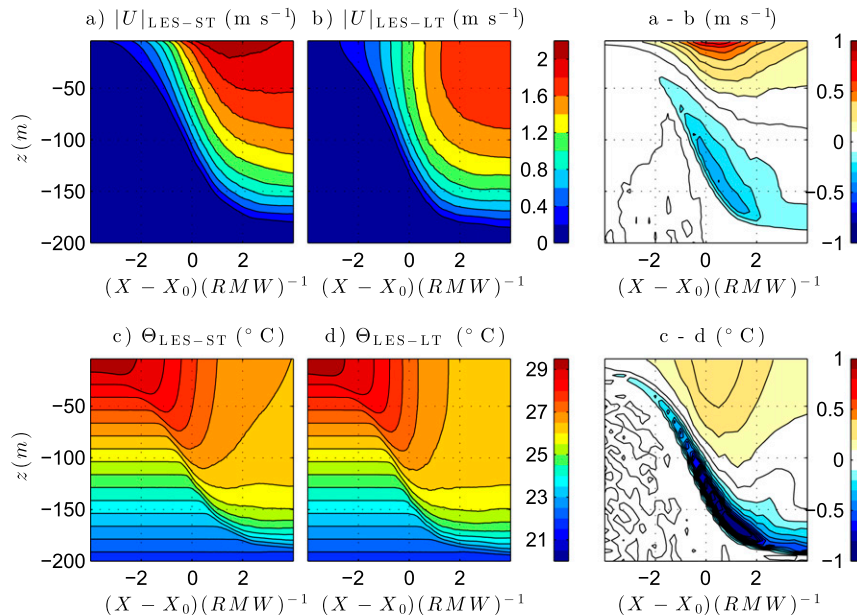
FIG. 3. LES transect (at 50 km to right of storm center) of (top) current magnitude and (bottom) temperature for a 5 m s^{-1} translating tropical cyclone. The results are shown for (left) LES–ST, (center) LES–LT, and (right) the difference between the two. The horizontal axes indicate the distance from the storm center position normalized by the RMW (50 km).

moving with the storm. Since our simulations are performed with a reasonably high spatial resolution in the direction perpendicular to the storm translation (Fig. 1), we can present the spatial snapshots of the current and temperature fields in Fig. 2. These spatial patterns remain independent of time after the wave field has reached quasi-steady state.

The contribution of Langmuir turbulence to cooling is greatest near the location of maximum Stokes drift shown in Fig. 1. The additional cooling due to Langmuir turbulence reaches a maximum of nearly 0.4°C on the right-hand side in a region where the total cooling is between 2.5° and 3°C. This is the region where the peak waves are longest and the Stokes drift penetrates deepest into the water column. This is also the location of rapid mixed layer deepening, suggesting that Langmuir turbulence is a significant contributor to the deepening of the mixing layer. The region of significant enhanced cooling (0.1°C or more) due to Langmuir turbulence is quite large, extending to about 3 (2) times the RMW to the right (left).

The near-surface current magnitude in LES–LT is smaller by as much as 0.7 m s^{-1} than that in LES–ST near the location of the maximum current. The Langmuir turbulence significantly increases the turbulent momentum transport within the upper portion of the water column where the Stokes drift and its vertical gradient are greatest. There is a small location near the center and in the left rear of the hurricane where the

currents are slightly stronger in the presence of Langmuir turbulence. Overall, Langmuir turbulence has a more noticeable impact on the mixing of currents than temperature in the upper water column, since the current gradients are strong, but temperature is well mixed and nearly uniform. This does not imply that the contribution to surface cooling is trivial, since even a temperature change of $O(0.1)$ °C may have significant implications for the tropical cyclone development (Emanuel 1999).

To demonstrate the vertical dependence of the Langmuir turbulence impact in this study, we present vertical transects of the upper-ocean current magnitude and temperature from 50 km to the right of the storm center (Fig. 3). The current is significantly decreased near the surface in LES–LT compared to the LES–ST in the area where the Stokes drift is large and the Langmuir turbulence is strong. The difference between the LES–LT and LES–ST currents decreases gradually from the surface down to about 50 m, suggesting that the impact of the Langmuir turbulence penetrates quite deep compared to the Stokes drift itself, which mostly decays within 10 m or so from the surface. Near the base of the mixing layer the LES–LT current is greater than the LES–ST currents, which is due to the increased mixing depth in LES–LT. The LES–LT temperature is cooler than the LES–ST temperature down to about 100 m, but there is less vertical dependence of the temperature difference compared to the current difference. At the
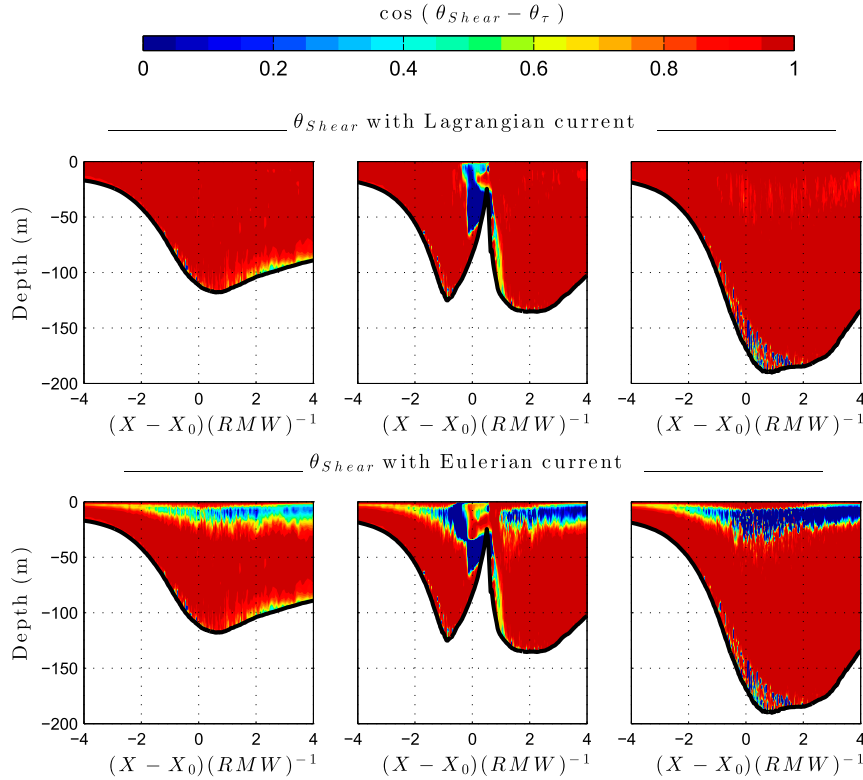
FIG. 4. Cosine of the misalignment angle between the directions of the Reynolds stress θ_τ and vertical gradient $\theta_{\partial\mathbf{U}_h/\partial z}$ of the (top) Lagrangian current and (bottom) Eulerian current for $5\,\mathrm{m\,s^{-1}}$, translating tropical cyclone from the LES–LT simulations. The test sites are from (left) 60 km to the left, (center) the storm center, and (right) 50 km to the right. The horizontal axis indicates the distance from the storm center position normalized by the RMW (50 km). Note that the color scale saturates at 0, but negative values can exist within the RMW. The solid black line represents the mixing layer depth using the bulk Richardson number criterion. Values beneath the mixing layer have been filtered out.

base of the mixing layer the LES–LT is warmer than LES–ST due to the increased mixing depth.

The LES–LT data are used to compare the direction of the turbulent Reynolds stress ($\overline{u'w'}$, $\overline{v'w'}$) with the Lagrangian and the Eulerian current shear directions (Fig. 4). It is clear that during the tropical cyclone passage the Reynolds stress aligns better with the Lagrangian shear throughout the entire mixing layer. There is a region of significant misalignment between the turbulent stress and the Eulerian shear in the upper 30 m. In this region, the Lagrangian shear is dominated by the Stokes drift shear, and the Eulerian shear is quite small. This suggests that the stress parameterization [Eq. (8)] based on the Lagrangian shear proposed by McWilliams et al. (2012) predicts the direction of the turbulent stress more accurately than the traditional parameterization based on the Eulerian shear under hurricane conditions.

During the passage of the hurricane eye there is strong misalignment of the turbulent stress from both the

Eulerian shear and the Lagrangian shear. This may be caused by strong disequilibrium of the turbulence in this region as the wind magnitude and direction rapidly change. Any turbulence closure models that assume alignment of stress and current shear may not perform well in these rapidly evolving conditions. To incorporate misaligned shear/stress in the KPP model requires the rotation of the stress from the shear direction to be included in the Reynolds stress calculation following McWilliams et al. (2012). That study shows that including the misalignment information obtained from a LES model improves the KPP performance. However, this is not a practical approach for tropical cyclone–ocean coupled forecast models.

5. Implicit Langmuir turbulence KPP model

Now that we have described the impact of Langmuir turbulence under tropical cyclones based on the LES results, we propose a modification to the KPP scheme

that can reproduce the LES–LT results in the one-dimensional model. This modification will proceed in the following manner. First, we demonstrate that the standard KPP scheme, which implicitly includes the typical (sea state independent) Langmuir turbulence impact, is not adequate to reproduce the simulated temperature and currents from the LES–LT (this section). Next, we remove the implicit Langmuir turbulence impact from the KPP model so that the one-dimensional simulation accurately reproduces the LES–ST results (section 6). We then introduce the explicit Langmuir turbulence impact in two steps. In step one, we replace the Eulerian current with the Lagrangian current in KPP because the LES results have clearly demonstrated that the turbulent fluxes are more closely aligned to the Lagrangian shear than the Eulerian shear. We find that this step does not produce enough mixing in the KPP model compared to the LES–LT (section 7). In step two, we introduce enhancement factors of the turbulent mixing coefficient and the unresolved shear in KPP so that the one-dimensional simulations best agree with the LES–LT results (section 8).

a. Method

We first investigate the performance of the standard KPP model (without explicit Langmuir turbulence effects) in tropical cyclone conditions. We define the standard KPP model following Large et al. (1994) in which the turbulent fluxes are calculated as the product of the eddy viscosity K_M (or diffusivity K_θ) and the mean vertical gradient of the momentum (or scalar) plus an additional nonlocal (countergradient) component [Eqs. (5) and (6)]. Because our experiments include only an insignificant surface buoyancy flux, the nonlocal components are neglected.

The vertical profile of K_x (where x can be θ or M) is a function of normalized depth $\sigma = -z/h$, where h is the mixing layer depth (which is defined for KPP later in this section). With the countergradient term dropped, $K_x(\sigma)$ is equal to the product of the mixing layer depth h, the turbulent velocity scale W_x, and a nondimensional shape function $G_x(\sigma)$:

$$K_x(\sigma) = h W_x G_x(\sigma). \qquad (15)$$

The nondimensional turbulent mixing shape function is approximated by a cubic polynomial $G_x(\sigma) = a_0 + a_1\sigma + a_2\sigma^2 + a_3\sigma^3$. The coefficients are determined following arguments of Large et al. (1994), where a_0 must be equal to zero (turbulent eddies do not cross the surface), a_1 equals one (to match the near-surface value of $K_x \sim -\kappa u_* z$), and a_2 and a_3 can be determined by matching the value and curvature of K_x to the interior. Since the interior turbulent

mixing parameter is negligible in this study, $a_2 \sim -2$ and $a_3 \sim 1$; thus, $G_x(\sigma) \sim \sigma(1 - \sigma)^2$ for both momentum and temperature. The turbulent velocity scale is $W_x = u_*\kappa/\phi_x(\sigma h/L)$, where κ is the von Kármán constant, ϕ_x is the universal stability function, and L is the Monin–Obhukhov length $u_*^3/(\kappa B_*)$. In this study, $L \gg h$ and $W_x \sim u_*\kappa$ for both momentum and temperature. Therefore, K_x, W_x, and G_x are all identical for temperature and momentum.

The mixing layer depth h is calculated by the KPP model using a bulk Richardson number Ri_b threshold, which compares the relative contribution of stabilizing buoyancy and destabilizing shear:

$$\text{Ri}_b(z) = \frac{[B^r - B(z)]|z|}{[U^r - U(z)]^2 + [V^r - V(z)]^2 + V_t^2(z)} < \text{Ri}_c, \qquad (16)$$

where B is the buoyancy, V_t is the unresolved turbulent velocity shear, and the superscript r denotes a reference value. At the bottom of the mixing layer $\text{Ri}_b(z = -h) = \text{Ri}_c$. The Ekman depth ($h_E \sim 0.7u_*/f$), which is important when stratification is weak, and the Monin–Obhukov depth ($h_{\text{MO}} = L = u_*^3/B_*\kappa$), which is important during surface heating (restratification) events, further restrict this mixing layer. The value of Ri_c varies based on the model resolution, but a typical value is 0.3. The unresolved turbulence term contains the contribution of convection to mixing:

$$V_t^2(z) = \frac{C_v(-\beta_T)^{1/2}}{\text{Ri}_c\kappa^2}(c_s\epsilon)^{-1/2}|z|NW_\theta, \qquad (17)$$

where N is the stability frequency and the constants are $C_v = 1.6$, $\beta_T = -0.2$, $c_s = 98.96$, and $\epsilon = 0.1$, following Large et al. (1994). This V_t^2 term should also include the unresolved Langmuir turbulence contribution to deepening the mixing layer (McWilliams et al. 2014). The reference variables in the bulk Richardson number (U^r, V^r, and B^r) are defined as the average over the upper 10% of the mixing layer, following Large et al. (1994) and Griffies et al. (2013). This averaging is a standard procedure because it reduces the resolution dependence of the bulk Richardson number. We also find that this averaging prevents overpredicting the mixing depth when the current is surface intensified, particularly under extreme wind speeds.

This version of KPP with $\text{Ri}_c = 0.3$ is defined as the implicit Langmuir turbulence (iLT) version for this study (hereinafter KPP–iLT) (see Table 2 for the list of all KPP experiment descriptions). It should be noted that this version of the model implicitly includes mean wave impacts (including Langmuir turbulence) because

TABLE 2. Description of various KPP model experiments.

KPP–iLT	KPP with implicit Langmuir turbulence.
KPP–ST	Retuned KPP to shear turbulence.
KPP–Lag	Retuned KPP with Lagrangian currents.
KPP–LT	Retuned KPP with Lagrangian currents and turbulent velocity-scale enhancement.

the coefficients (particularly Ri_c) have been determined empirically from in situ data and the real ocean always contains waves when there is significant wind.

b. Results

We first compare the mean near-surface ($z = -5$ m) values of both temperature anomaly (where the initial temperature is subtracted from the simulated temperature) and currents. We evaluate the results at the near-surface since this is most relevant for the hurricane modeling application, but the conclusions are essentially the same if we choose a deeper ($z = -30$ m) transect for comparison. The root-mean-square difference between the KPP (one-dimensional GOTM) and LES results is used as a metric to evaluate the KPP performance. RMS difference is computed over 24 h (± 12 h relative to the passage of the peak winds) in all test experiments (both translation speeds, both initial mixed layer depths) and at all locations. For the 5 m s^{-1} translating storm this corresponds to the spatial study transect of 432 km, and for the 10 m s^{-1} translating storm this corresponds to the spatial study transect of 864 km. As long as the time and location are consistent, this is a useful metric to compare different KPP methods within this study. Note that because both the LES and the one-dimensional model are initialized with zero mean current, the phases of the inertial oscillations remain almost identical between the two models.

The results of the KPP–iLT and LES–LT experiments are compared in Fig. 5. All results (both initial mixed layer depths and both translation speeds) are included in the left panels. The small difference in the temperature anomaly between KPP–iLT and LES–LT (less than 0.1°C at most locations) suggests KPP–iLT does a reasonable job predicting the mean mixing layer depth and surface cooling over the range of Langmuir turbulence conditions under the tropical cyclones. KPP–iLT gives a slight warm bias (Fig. 5, bottom-center and bottom-right panels), but this bias could be corrected by adjusting the critical Richardson number. The cooling on the left-hand side of the 5 m s^{-1} moving tropical cyclone is noticeably underpredicted, which is discussed further in the following section.

The currents predicted by KPP–iLT are much different from those predicted by LES–LT. The error is almost as large as the contribution of Langmuir turbulence

itself shown in Fig. 2. This suggests that increased near-surface mixing from Langmuir turbulence is not captured well by KPP–iLT and that accurate current predictions require introducing explicit Langmuir turbulence effects in the KPP model. In the upper-left panel, the time history of the current magnitude at each LES location can be seen. Initially, both LES–LT and KPP–iLT currents are zero. They increase and diverge as the wind and Stokes drift increase and the Langmuir turbulence becomes more important. They eventually converge as the wind decreases and the turbulent mixing becomes less important. Part of the difference between the KPP–iLT current and the LES–LT current is due to the presence of the Stokes drift itself. Since the turbulent mixing occurs in response to the Lagrangian shear in LES–LT, the behavior of the Lagrangian current in LES–LT is more similar to the behavior of the Eulerian current in KPP–iLT. Nevertheless, the difference between the KPP–iLT current and the LES–LT current remains significant even below the depth of significant Stokes drift because of the enhanced Langmuir turbulence mixing.

6. Shear turbulence KPP without wave effects

a. Method

Before introducing explicit Langmuir turbulence effects to rectify the underprediction of mixing in the KPP model, it is necessary to remove the implicit wave impacts that are already included in KPP–iLT. To remove the implicit Langmuir turbulence, we retune the critical Richardson number by optimizing (reducing) the near-surface RMS difference of temperature and current between the one-dimensional simulations and the LES–ST results. An alternative way to retune the KPP model would be to keep the critical Richardson number unchanged and to reduce the turbulent velocity scale W_x at large Langmuir numbers (to reduce the shear-driven turbulence). This method, however, is not consistent with the traditional near-surface wall layer turbulence $W_x \sim \kappa u_*$ and does not yield good performance in the KPP model. We find that the retuned critical Richardson number of 0.235 gives optimal agreement between the KPP and the LES–ST results for surface temperature anomaly and currents. Interestingly, this is also similar to the value of 0.25 found for atmospheric boundary
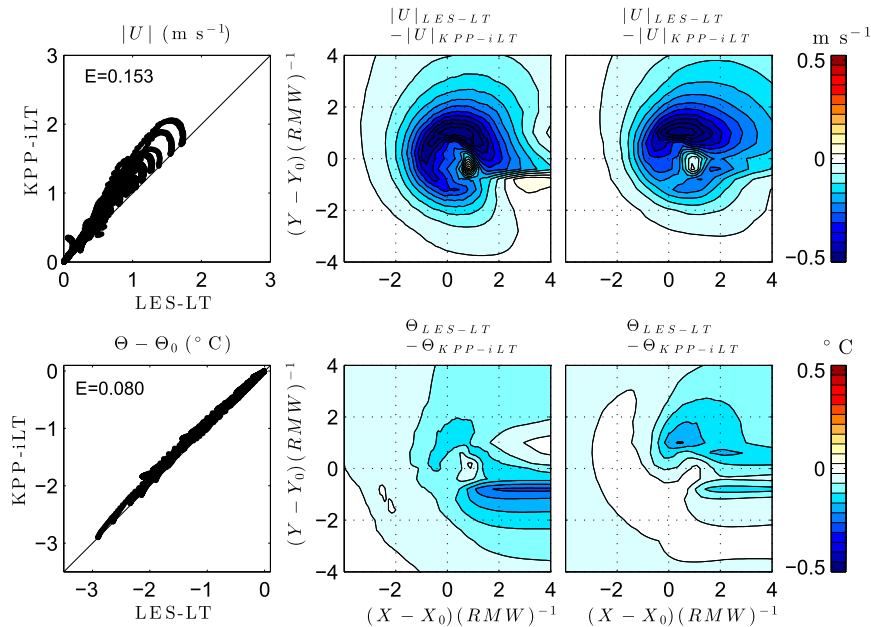
FIG. 5. Results of (top) current magnitude and (bottom) temperature anomaly (temperature minus initial temperature) at 50-m depth. (left) Results from the one-dimensional model with the KPP–iLT on the vertical axis vs results from the LES–LT model on the horizontal axis. The "E" value is the RMS difference. (center) Difference between results from KPP–iLT and LES–LT for the $5 \, \mathrm{m \, s^{-1}}$ translating tropical cyclone. The horizontal and vertical axes indicate the distance from the storm center position normalized by the RMW (50 km). (right) As in the (center), but for the $10 \, \mathrm{m \, s^{-1}}$ translating tropical cyclone.

layer closure schemes similar to the KPP (see, e.g., Hong and Pan 1996). This version of the KPP model is hereinafter called KPP–ST.

b. Results

The results of the KPP–ST and LES–ST experiments are compared (Fig. 6) in the same manner as the previous section. The RMS difference for both near-surface current and temperature anomaly are considerably reduced across the range of forcing parameters in this experiment as a result of modifying the critical Richardson number.

As in the case of KPP–iLT (Fig. 5), the cooling on the left-hand side of the $5 \, \mathrm{m \, s^{-1}}$ moving tropical cyclone is noticeably underpredicted (Fig. 6, lower-middle panel). This problem is clearly unrelated to the Langmuir turbulence. It is rather related to KPP's shortcoming in handling the rapidly changing wind forcing. When the wind speed rapidly decreases after the storm passage, the near-surface current rapidly decreases as well. The KPP model predicts a shallower mixing layer depth based on the critical Richardson number criterion, and the deepening of the mixing layer ceases. However, the LES model shows that the turbulence near the bottom of the mixing layer does

not weaken as rapidly and the mixing layer continues to deepen during this phase of the tropical cyclone. The KPP fails to accurately predict the vertical variation of the turbulence in such a transient and non-equilibrium condition. The problem is more evident on the left-hand side because the mixing layer is much shallower and the sea surface temperature is more sensitive to the underprediction of the mixing layer deepening. Because this is not related to the Langmuir turbulence effect in the KPP model, we do not address it any further in this study.

7. KPP with Lagrangian currents

a. Method

Before adding the explicit Langmuir turbulence parameterization into the KPP–ST model, we consider the effect of the Lagrangian shear (with the Stokes drift) in place of the Eulerian shear. Figure 4 indicates a better alignment between the Reynolds stress and the Lagrangian shear. In all diffusion equations the current shear is replaced with the Lagrangian shear as shown in Eq. (8). In addition, the bulk Richardson number calculation is modified to account for the Lagrangian (Lag) shear:
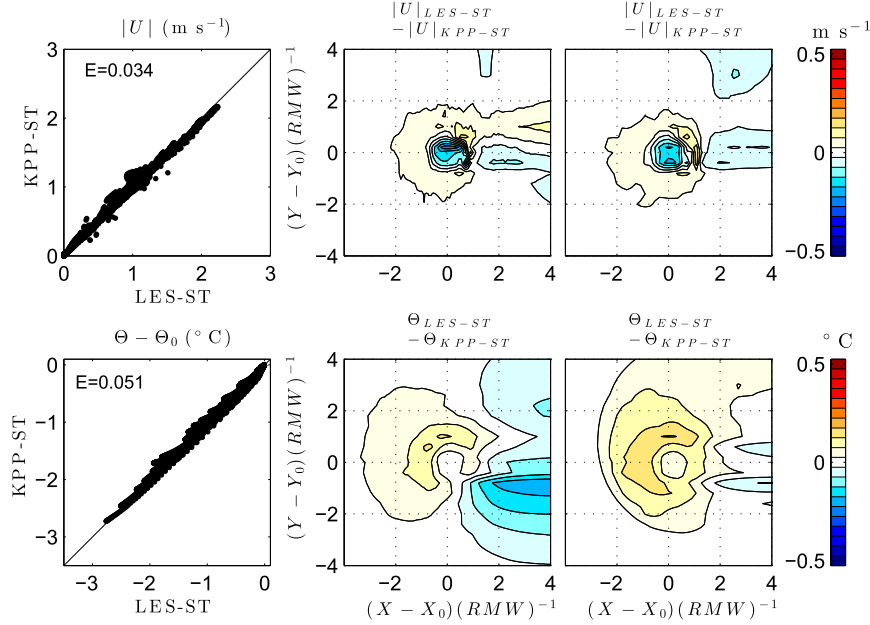
FIG. 6. As in Fig. 5, but KPP–ST is compared to LES–ST.

$$\mathrm{Ri}_b(z) = \frac{[B^r - B(z)]|z|}{[U_L^r - U_L(z)]^2 + [V_L^r - V_L(z)]^2 + V_t^2(z)} < \mathrm{Ri}_c,$$
(18)

with the critical Richardson number fixed at 0.235 as in the KPP–ST. This version of the KPP model is hereinafter called KPP–Lag.

b. Results

We now compare the results of the KPP–Lag and LES–LT experiments to test the performance of the KPP model using the Lagrangian currents (Fig. 7). Clearly, KPP–Lag improves the current predictions relative to KPP–iLT under a tropical cyclone. However, there is now significantly more undercooling relative to KPP–iLT. This suggests that the mixed layer deepening and entrainment are underpredicted, since the surface heat flux is omitted in this study.

To investigate the cause of the undermixing, we compare the mixing coefficient K_M in KPP–Lag and the mixing coefficient K_{LES} that is directly estimated from the LES–LT results. Since the Lagrangian shear and the stress are mostly aligned, the K_{LES} is derived as follows:

$$K_{\mathrm{LES}} = \frac{|\overline{u'w'} + i\overline{v'w'}|}{\left|\frac{\partial U_L}{\partial z} + i\frac{\partial V_L}{\partial z}\right|}.$$
(19)

The mixing layer depth h is also required to obtain a nondimensional mixing coefficient profile $G(\sigma)_{\mathrm{LES}} = K_{\mathrm{LES}}/(\kappa u_* h)$ from the LES results. The mixing layer depth h is determined by applying the same bulk Richardson number threshold [Eq. (18)], with the critical value of 0.235, to the LES mean field.

Examples comparing the nondimensional mixing coefficient profiles $G_M(\sigma)$ and $G(\sigma)_{\mathrm{LES}}$ at locations to the left and right of the storm track are presented in Fig. 8 (from a tropical cyclone experiment with a 5 m s^{-1} translation speed and a 10-m initial mixed layer depth). These examples are from (upper panels) 4 h prior to maximum wind, (middle panels) the time of maximum wind, and (lower panels) 4 h after the maximum wind. The LES profiles (black dots) show a clear enhancement of the mixing coefficient in the presence of Langmuir turbulence, which is missing in KPP–Lag (red line).

This analysis supports previous efforts (McWilliams and Sullivan 2000) of enhancing the mixing coefficient in the KPP model that varies with the Langmuir number. In the next section, we will explore different ways of enhancing the mixing coefficient in the KPP–Lag model.

8. KPP with Lagrangian currents and enhanced mixing

a. Method

In the KPP model, the enhancement to the turbulent mixing coefficient can be introduced through a factor F_{LT}:

$$K_x^{\mathrm{LT}} = K_x F_{\mathrm{LT}},$$
(20)

where K_x is defined by Eq. (15). The unresolved turbulent shear contribution V_t^2 [Eq. (17)] must also be modified to
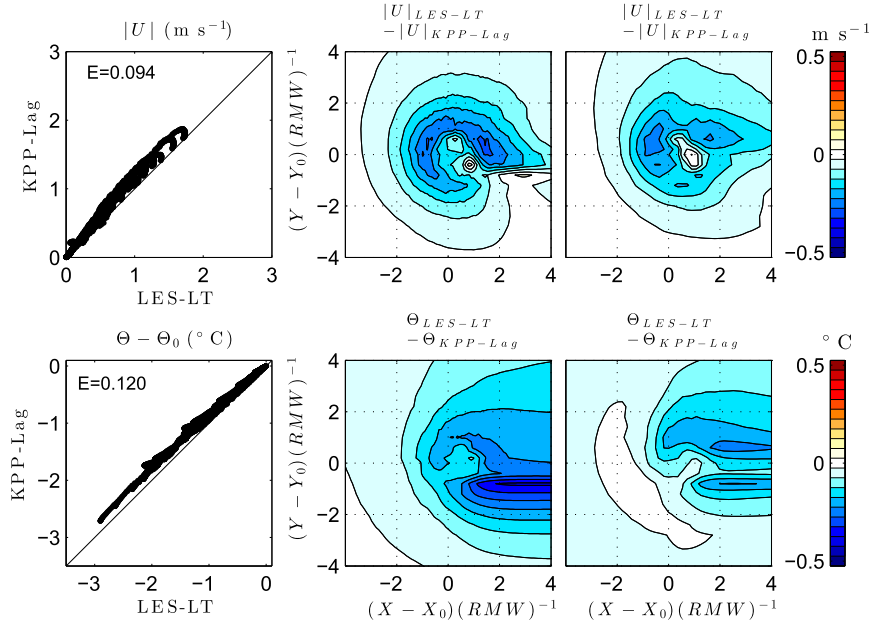
FIG. 7. As in Fig. 5, but KPP–Lag is compared to LES–LT.

account for the contribution of Langmuir turbulence (following McWilliams et al. 2014):

$$(V_t^{\mathrm{LT}})^2 = V_t^2 F_{\mathrm{LT}}^{Vt}. \qquad (21)$$

We differentiate between the enhancement to the unresolved shear contribution F_{LT}^{Vt} and F_{LT} used in the mixing coefficient profile for reasons that will be discussed later in this section.

In previous studies the enhancement factor F_{LT} has been determined as a function of the turbulent Langmuir number (McWilliams and Sullivan 2000; Van Roekel et al. 2012). However, the definition of the turbulent Langmuir number itself varies from study to study and requires some consideration. McWilliams and Sullivan (2000) define the turbulent Langmuir number based on the surface Stokes drift:

$$\mathrm{La}_t = \sqrt{\frac{u_*}{|\mathbf{u}_S(z=0)|}}, \qquad (22)$$

which is valid for aligned wind and waves. Another proposed form, which also applies to the aligned case only, is

$$\mathrm{La}_{\mathrm{SL}} = \sqrt{\frac{u_*}{\langle|\mathbf{u}_S|\rangle_{\mathrm{SL}}}}, \qquad (23)$$

where $\langle|\mathbf{u}_S|\rangle_{\mathrm{SL}}$ is the Stokes drift magnitude averaged over the surface layer, which is defined as the top 20%

of the mixed layer (Harcourt and D'Asaro 2008). In Harcourt and D'Asaro (2008), the surface layer–averaged Stokes drift is referenced to the Stokes drift at the base of the mixed layer, but we find this does not significantly impact the results because of the large mixed layer depths observed in this study. We have therefore approximated this reference Stokes drift as 0, though this simplification may not be appropriate for nonhurricane conditions. The averaging over the surface layer is performed because it is unlikely that the waves that decay within the first few meters contribute significantly to the Langmuir turbulence on scales relevant to the mixed layer. Van Roekel et al. (2012) have further modified the Langmuir number definition to accommodate misaligned wind and waves:

$$\mathrm{La}_{\mathrm{SL}\theta} = \sqrt{\frac{u_* \cos(\theta_{\mathrm{Wind}} - \theta_{\mathrm{Lag}})}{\langle|\mathbf{u}_S|\rangle_{\mathrm{SL}} \cos(\theta_{\mathrm{Waves}} - \theta_{\mathrm{Lag}})}}, \qquad (24)$$

where θ_{Wind} is the wind direction, θ_{Waves} is the direction of the average Stokes drift, and θ_{Lag} is the direction of the Lagrangian shear over the surface layer. They also suggest that the surface layer depth should be defined as the top 20% of the mixing layer rather than the mixed layer. The directional components define the projection of the wind and the Stokes drift into the mean Lagrangian shear direction (used as a proxy for dominant Langmuir turbulence eddy orientation). Note that this form
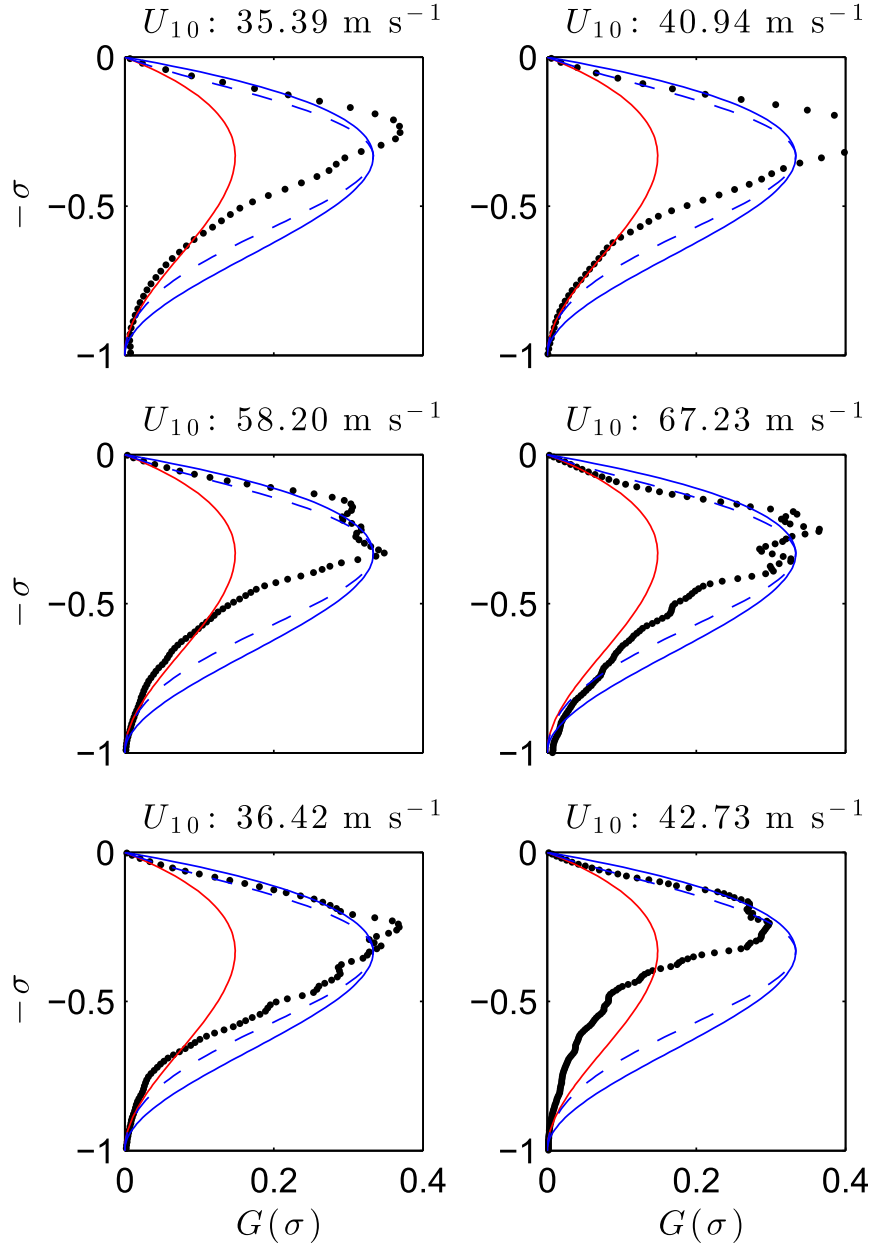
FIG. 8. Vertical profile of nondimensional mixing coefficient at (top) 4 h prior to peak wind, (middle) peak wind, and (bottom) 4 h after peak wind at locations (left) −40 and (right) +50 km as derived from the LES turbulent stress (black dots) compared to the parameterized profile in the KPP model without any enhancement (solid red) and with the enhancement proposed in Eq. (27) (solid blue). The dashed blue shows the KPP model result where the enhancement is reduced near the surface and near the base of the mixed layer [Eq. (30)].

may yield a very small Langmuir number (strongly enhanced Langmuir turbulence) if the Lagrangian shear is significantly misaligned with wind, which is not observed in our LES experiments. Furthermore, this Langmuir number is undefined if $|\theta_{\mathrm{Waves}} - \theta_{\mathrm{Lag}}|$ exceeds $\pi/2$. Although such conditions rarely occur, it is important to

remove the nonphysical Langmuir number in complex wind and wave conditions under a tropical cyclone.

In this study we find that the misalignment between the wind and the Lagrangian shear is negligible [$\cos(\theta_{\mathrm{Wind}} - \theta_{\mathrm{Lag}}) \approx 1$]. Therefore, for simplicity we neglect this effect and modify the definition of the Langmuir number to
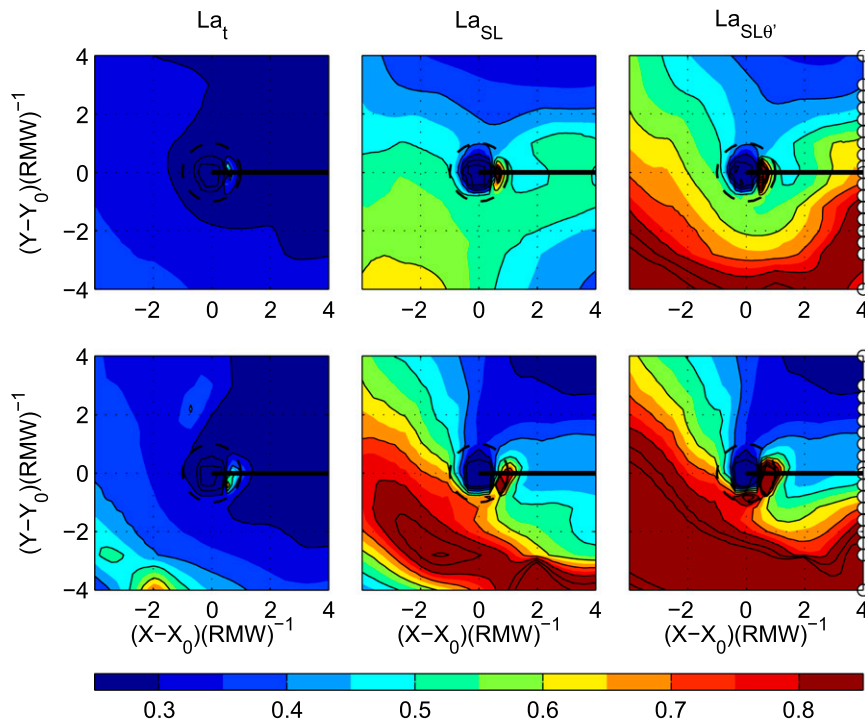
FIG. 9. Spatial distribution of Langmuir number for a (top) 5 and (bottom) $10 \, \mathrm{m \, s^{-1}}$ translating tropical cyclone. The horizontal and vertical axes indicate the distance from the storm center position normalized by the RMW (50 km). (left) La_t [Eq. (22)] based on the surface Stokes drift (lower wavelength limit of 1 m), (center) $\mathrm{La}_{\mathrm{SL}}$ [Eq. (23)] based on the surface layer–averaged (top 20% of the mixing layer) Stokes drift, and (right) $\mathrm{La}_{\mathrm{SL}\theta'}$ [Eq. (25)] based on the surface layer–averaged Stokes drift and corrected for misalignment between current shear and waves. The white open circles in the right panels show the test site locations. The color scale saturates above 0.8, but the Langmuir number can be much larger when the Stokes drift is small and/or the wind stress is large.

$$\mathrm{La}_{\mathrm{SL}\theta'} = \sqrt{\frac{u_*}{\langle |\mathbf{u}_S| \rangle_{\mathrm{SL}}} \frac{1}{\max[\cos(\theta_{\mathrm{Waves}} - \theta_{\mathrm{Lag}}), 10^{-8}]}}, \quad (25)$$

that is, the misalignment between the waves, and the Lagrangian shear is limited to $\pi/2$ in the Langmuir number calculation. We also define the surface layer as the top 20% of the mixing layer instead of the mixed layer. Note that when the misalignment between the waves (Stokes drift) and the Lagrangian shear exceeds $\pi/2$, there is a possibility that the upper-ocean turbulence is suppressed instead of enhanced due to surface waves (Rabe et al. 2015), that is, the enhancement factor may become less than 1. However, we find that such occurrences are rare (short lived at a particular location) and do not significantly affect the mixed layer deepening process. Therefore, we do not find it necessary to accommodate such cases in the modified KPP model.

The three forms of the Langmuir number are compared in Fig. 9. At the surface, all resolved spectral

wavenumbers ($k \leq k_{\mathrm{UL}}$) contribute to the Stokes drift. The decay rate is an exponential function of the wavenumber so that waves shorter than 10 m decay to less than 10% of their surface value by $z = -2 \, \mathrm{m}$. This means a larger magnitude for the surface-based definition of the Stokes drift (La_t, left panels) and thus smaller Langmuir number. The center panel shows the surface layer–averaged definition $\mathrm{La}_{\mathrm{SL}}$, where the surface layer is defined as the top 20% of the mixing layer. This Langmuir number is weighted toward the magnitude of longer waves that contribute to the Stokes drift over a larger fraction of the mixing layer. The projected surface layer–averaged Langmuir number ($\mathrm{La}_{\mathrm{SL}\theta'}$, right panels) gives significantly higher values than $\mathrm{La}_{\mathrm{SL}}$ when the Lagrangian shear becomes misaligned with the waves, mainly on the left of the storm and near the eye. For the transient, turning wind in a moving tropical cyclone, the projected definition of the Langmuir number is likely more desirable. We have also tested the projected Langmuir number $\mathrm{La}_{\mathrm{SL}\theta}$ and have found that the results

are almost identical to the $\text{La}_{\text{SL}\theta'}$ except for very small areas (mainly inside the RMW) where $\text{La}_{\text{SL}\theta'}$ becomes extremely small or undefined.

Next, we consider the enhancement factor F_{LT} to the turbulent eddy viscosity (or diffusivity) K_x as a function of the turbulent Langmuir number. There have been many previous attempts to scale the enhancement of the vertical velocity variance $\langle w'^2 \rangle$ (averaged over the entire mixing layer or mixed layer) normalized by the friction velocity squared and the enhancement factor F_{LT} in the KPP model. Some LES studies support the scaling argument based on the ratio of the Stokes production to the dissipation and suggest $\langle w'^2 \rangle \propto u_*^2 \text{La}_t^{-4/3}$ (Min and Noh 2004; Harcourt and D'Asaro 2008; Grant and Belcher 2009; McWilliams et al. 2014), when the Stokes production is significant (small Langmuir numbers). McWilliams and Sullivan (2000) suggest an enhancement factor of $F_{\text{LT}} = (1 + 0.08\text{La}_t^{-4})^{1/2}$. Recently, Van Roekel et al. (2012) have introduced a new scaling based on the projected Langmuir number:

$$\frac{\langle w'^2 \rangle}{u_*^2 \, \cos^2(\theta_{\text{Wind}} - \theta_{\text{Lag}})} = 0.6[1 + (1.5\text{La}_{\text{SL}\theta})^{-2} + (5.4\text{La}_{\text{SL}\theta})^{-4}]. \tag{26}$$

While the enhancement of $\langle w'^2 \rangle / u_*^2$ and the enhancement factor F_{LT} should be related, the exact relationship between the two is not trivial. This is because the Langmuir turbulence likely modifies not only the velocity scale, but also the length scale in the KPP model. In this study, we do not attempt to separate these two contributions but rather focus on the total combined impact on the mixing coefficient. We also separate the enhancement of the mixing coefficient F_{LT} and the enhancement of the unresolved turbulent shear contribution F_{LT}^{Vt} because these two may be related to different length and velocity scales.

Since there is no general consensus regarding the form of F_{LT}, we determine the enhancement factor empirically by using the LES experimental results. As described in the previous section, a nondimensional mixing coefficient profile $G(\sigma)_{\text{LES}} = K_{\text{LES}}/(\kappa u_* h)$ can be obtained from the LES results. The maximum value of $G(\sigma)_{\text{LES}}$ within the mixing layer is then compared to the maximum value of $G_M(\sigma)$ that is used by the KPP model {i.e., $\max[G_M(\sigma)] \sim \max[\sigma(1 - \sigma)^2] \sim 0.1481$ for $0 \leq \sigma \leq 1$}. The ratio of these quantities is the LES enhancement factor that should be consistent with F_{LT} in the modified KPP model. In addition, the LES vertical velocity variance $\langle w'^2 \rangle$ is readily available from the LES results, and the

enhancement of $\langle w'^2 \rangle / u_*^2$ can be compared to the LES enhancement factor.

First, it is beneficial to perform this exercise using the LES–ST experiments to confirm that the KPP–ST K_M profile agrees with the K_{LES} profile derived from the LES–ST. In this case, the Lagrangian current is equal to the Eulerian current in Eqs. (18) and (19). The calculated LES enhancement factor {$F_{\text{LT}}^{\text{LES}} = \max[G(\sigma)_{\text{LES}}]/0.1481$, the ratio of the maximum value of $G(\sigma)_{\text{LES}}$ to 0.1481} is 0.81 ± 0.20 (the latter number is the standard deviation over $n = 6337$) for all times and locations except with wind speed less than $5 \, \text{m s}^{-1}$ and the locations inside the RMW. These results suggest that the KPP mixing coefficient is indeed consistent with the effective mixing coefficient in the LES without wave effects (no Langmuir turbulence), as expected from the good agreement between the KPP–ST and LES–ST results, except for very low-wind conditions and very complex wind conditions inside the RMW.

Figure 10 shows the LES enhancement factor (ratio of maximum normalized LES mixing coefficient to maximum normalized KPP mixing coefficient) as a function of the surface layer–averaged Langmuir number La_{SL} (middle-left panel) and the projected surface layer Langmuir number $\text{La}_{\text{SL}\theta'}$ (lower-left panel) for all LES experiments with waves. The results are distinguished by different colors depending on the locations relative to the storm. The projected Langmuir number reduces scatter relative to the surface Langmuir number. The improvement is most prevalent on the left-hand side of the storm where wind-wave misalignment occurs more often. The LES enhancement factor clearly exceeds 1 at most locations, suggesting that Langmuir turbulence does indeed enhance the mixing coefficient. By bin averaging our data, we find that the LES enhancement factor scales well with a simple empirical form of

$$F_{\text{LT}} = 1 + \text{La}_{\text{SL}\theta'}^{-1}, \tag{27}$$

shown by a solid black line, for Langmuir numbers above 0.8. The mixing coefficient enhancement appears to level off around 2.25 for Langmuir numbers below 0.8, possibly even decaying for lower Langmuir numbers. This is qualitatively consistent with McWilliams et al. (2014), who also find that the eddy viscosity magnitude decreases at very low Langmuir numbers. However, after close examination we have found that the leveling off or reduction of the enhancement factor only occurs in the rear right of the storm, where the mixing layer depth h can be significantly overestimated based on the Richardson number criterion applied to the LES results. It is likely that the overestimation of h contributes to the apparent
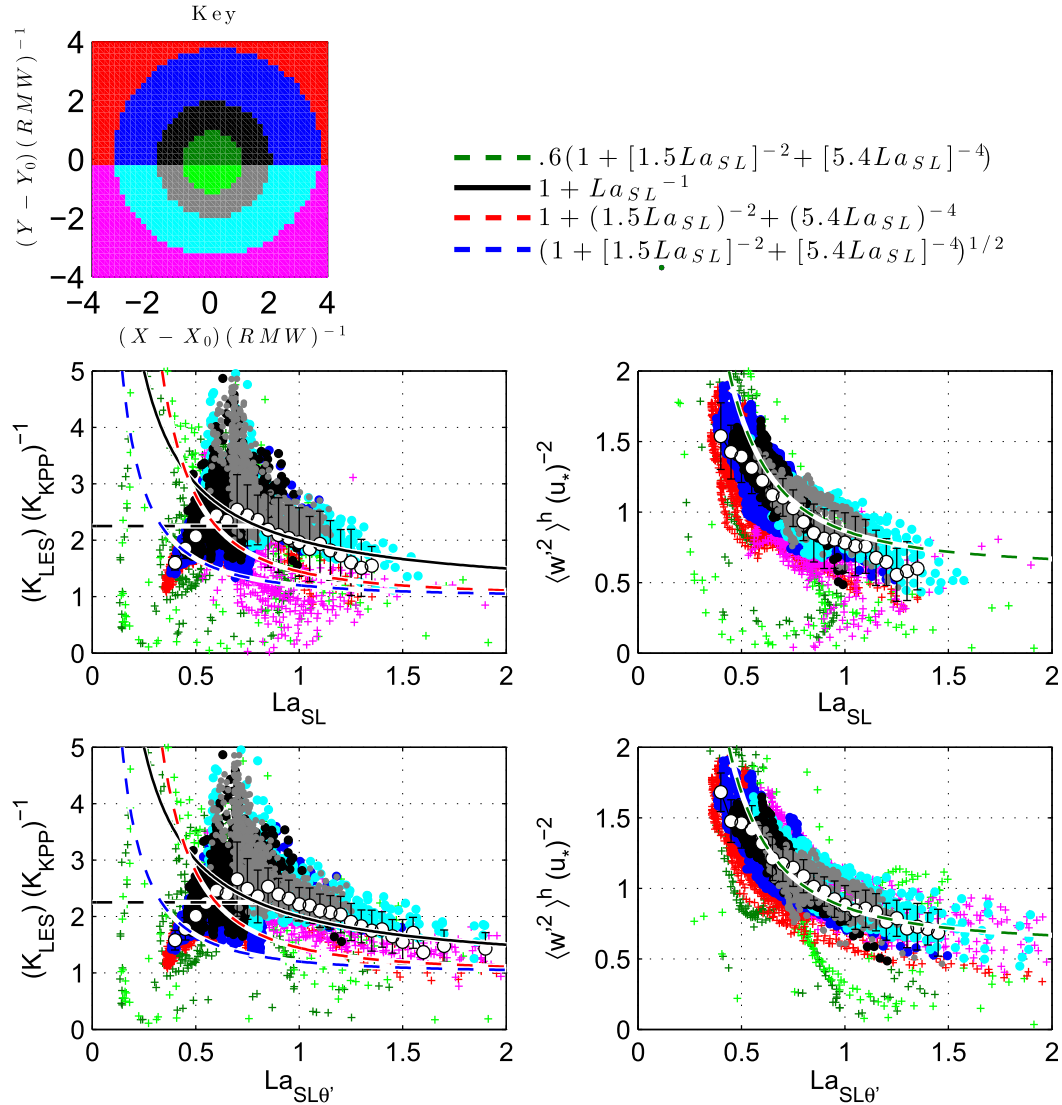
FIG. 10. (left) LES enhancement factor (ratio of maximum normalized LES mixing coefficient to maximum normalized KPP mixing coefficient) and (right) mixing layer–averaged vertical velocity variance scaled by the friction velocity squared. Both quantities are plotted against (top) the surface layer Langmuir number La_{SL} and (bottom) the surface layer projected Langmuir number $La_{SL\theta'}$. The marker color locations are given in the map at the top. White circles with vertical bars are bin averages with standard deviations. (The lines labeled in the legends are described in the text.)

reduction of the LES enhancement factor. Because of this uncertainty we cap the empirical enhancement factor at 2.25 for Langmuir numbers below 0.8 as shown by the dashed black line.

Next, we examine the enhancement of $\langle w'^2 \rangle / u_*^2$ directly obtained from the LES results (right panels). This exercise further demonstrates the importance of the misalignment correction of the Langmuir number, supporting the results of Van Roekel et al. (2012) and Rabe et al. (2015). It is interesting that the scaling of Van Roekel et al. (2012) [Eq. (26) with

$\cos(\theta_{\mathrm{Wind}} - \theta_{\mathrm{Lag}}) = 1$; green dashed line in Fig. 10] is a very good fit to our LES results as well. We have also found that our LES–ST results yield $\langle w'^2 \rangle / u_*^2 = 0.57 \pm 0.24$, which is consistent with the large Langmuir number limit of 0.6 by Van Roekel et al. (2012). At very low Langmuir numbers the LES $\langle w'^2 \rangle / u_*^2$ starts to deviate from the scaling of Van Roekel et al. (2012), possibly because of the overestimation of h as discussed earlier. If h is overestimated, the mixing layer average of $\langle w'^2 \rangle$ is performed including a region of weak turbulence below the real mixing layer and the result may be underestimated.

We do not compare our results with the enhancement factor given by McWilliams and Sullivan (2000) since their form was obtained using the very different Langmuir number La$_t$ based on the surface Stokes drift. The scaling of $\langle w'^2 \rangle / u_*^2$ presented in Harcourt and D'Asaro (2008) avoids the asymptotic breakdown as La $\to 0$ (see McWilliams and Sullivan 2000; Harcourt and D'Asaro 2008), unlike the scaling of Van Roekel et al. (2012). However, the difference between these two is appreciable only at very low Langmuir numbers where our results are not reliable. We also note that the values of $\langle w'^2 \rangle$ can be quite different if the averaging is done over the entire mixed layer (Van Roekel et al. 2012; Rabe et al. 2015) instead of the entire mixing layer (this study).

We now investigate the relationship between the LES enhancement factor and the enhancement of $\langle w'^2 \rangle / u_*^2$. If we assume that the length scale of the KPP mixing coefficient K_M is not affected by the Langmuir turbulence and the velocity scale of K_M is enhanced in the same manner as the square root of the vertical velocity variance $\langle w'^2 \rangle$, the enhancement factor F_{LT} should be identical to the square root of $\langle w'^2 \rangle / u_*^2$ divided by its limiting value at large Langmuir numbers (no Langmuir turbulence). Then, the scaling by Van Roekel et al. (2012) [Eq. (26)] suggests that

$$F_{\mathrm{LT}} = [1 + (1.5\mathrm{La}_{\mathrm{SL}\theta})^{-2} + (5.4\mathrm{La}_{\mathrm{SL}\theta})^{-4}]^{1/2}. \quad (28)$$

However, this scaling significantly underestimates the LES enhancement factor (blue dashed line in the left panels of Fig. 10). If we instead assume that F_{LT} is identical to the enhancement to $\langle w'^2 \rangle / u_*^2$, the scaling of Van Roekel et al. (2012) suggests

$$F_{\mathrm{LT}} = 1 + (1.5\mathrm{La}_{\mathrm{SL}\theta})^{-2} + (5.4\mathrm{La}_{\mathrm{SL}\theta})^{-4}. \quad (29)$$

This scaling (red dashed line in the left panels) is more consistent in terms of the order of magnitude but still underestimates the LES enhancement factors except for very low Langmuir numbers. These exercises suggest that the enhancement to the velocity and length scales of K_M is not simply related to the enhancement of the vertical velocity variance $\langle w'^2 \rangle$ and support our approach of determining F_{LT} empirically.

The ratio of K_M and K_{LES} is not constant with depth (see Fig. 8). Comparing many similar profiles, we find that this ratio roughly peaks at the maximum of the K_M profile and approaches 1 at the top and bottom boundaries. For that reason we apply the enhancement factor at its maximum where the nondimensional profile also reaches its maximum. The enhancement factor is

then reduced to 1 approaching both the top and bottom boundaries.

In summary, based on this analysis, we set our KPP Langmuir turbulence enhancement factor F_{LT}^K as

$$F_{\mathrm{LT}}^K(\sigma) = 1 + (F_{\mathrm{LT}}' - 1)G_x(\sigma)/\max[G_x(\sigma)], \quad (30)$$

$$F_{\mathrm{LT}}' = 1 + \mathrm{La}_{\mathrm{SL}\theta'}^{-1}, \quad \mathrm{La}_{\mathrm{SL}\theta'} \geq 0.8, \quad (31)$$

(black solid line in Fig. 10) and

$$F_{\mathrm{LT}}' = 2.25, \quad \mathrm{La}_{\mathrm{SL}\theta'} \leq 0.8, \quad (32)$$

(black dashed line in Fig. 10). Referring back to Fig. 8, the KPP profile with the enhancement (blue) clearly does a better job reproducing the LES turbulent mixing coefficient profile compared to the KPP profile without the enhancement (red). The impact of reducing the enhancement toward the bottom and the top (blue dashed) greatly improves agreement near the surface and helps avoid overentrainment of cool water at the base of the mixing layer.

We find that using the same form of the enhancement factor in both the turbulent mixing profile K_x and the unresolved shear V_t does not work. This supports the conclusion of McWilliams et al. (2014) that the scale of Langmuir turbulence that contributes to the near-surface mixing is different from the scale of Langmuir turbulence that drives mixed layer deepening. The deepening of the mixing layer (the contribution of Langmuir turbulence to the V_t term) is underpredicted if the same enhancement factor [Eqs. (31) and (32)] is used. To address this, we empirically modify the enhancement factor for V_t to

$$F_{\mathrm{LT}}^{Vt} = 1 + 2.3\mathrm{La}_{\mathrm{SL}\theta'}^{-1/2} \quad (33)$$

so that the bulk Richardson number calculation is now

$$\mathrm{Ri}_b(z) = \frac{[B^r - B(z)]|z|}{[U_L^r - U_L(z)]^2 + [V_L^r - V_L(z)]^2 + [V_t(z)F_{\mathrm{LT}}^{Vt}]^2}. \quad (34)$$

This form [Eq. (33)] was found by optimizing the agreement between the one-dimensional model and the LES results of mixing layer depth evolution and surface cooling, by varying both the slope and magnitude of the enhancement factor while maintaining that the enhancement factor approaches one in the large Langmuir number limit.

The KPP model with the Lagrangian shear (instead of the Eulerian shear) and with the enhancement factors, in the form of Eqs. (30)–(32) for K_x and Eq. (33) for V_t, is hereinafter called KPP–LT.
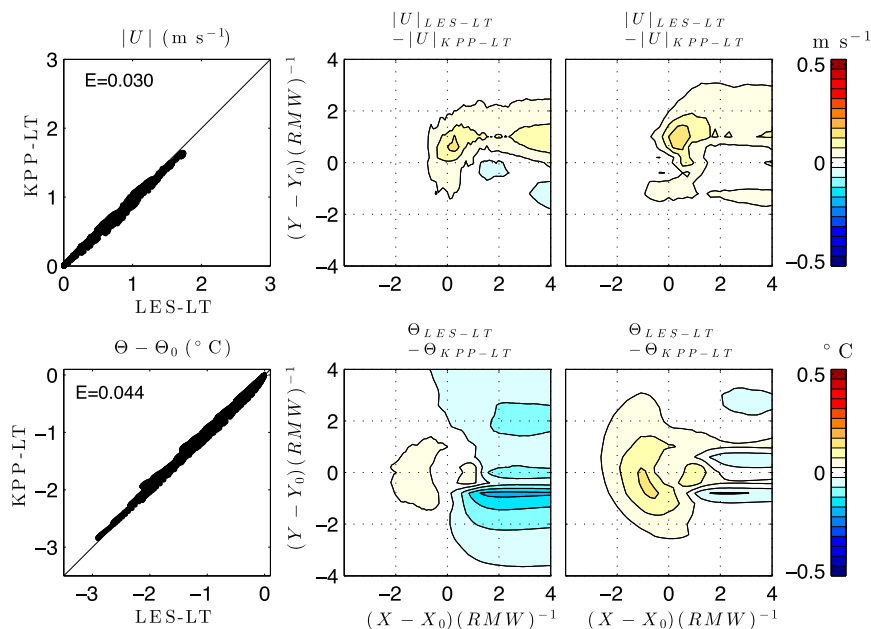
FIG. 11. As in Fig. 5, but KPP–LT is compared to LES–LT.

b. Results

The results of the comparison of the KPP–LT experiment against the LES–LT experiment (Fig. 11) show much improved agreement compared to the KPP–iLT experiment (Fig. 5). Most noticeably, the prediction of the near-surface current has improved from a RMS difference of $0.153\,\mathrm{m\,s^{-1}}$ (with local differences greater than $0.5\,\mathrm{m\,s^{-1}}$) to a much reduced RMS difference of $0.030\,\mathrm{m\,s^{-1}}$ (with local differences smaller than $0.15\,\mathrm{m\,s^{-1}}$). Even as the eye of the storm passes, the prediction of the cooling remains within 0.1°C of the LES–LT results in the center. After the eye has passed, some undercooling in the KPP–LT experiment is noticeable particularly on the left-hand side. However, this corresponds to the region where the KPP performs even worse in shear-only turbulence experiments, as discussed in section 6.

We have also conducted identical experiments with slightly different enhancement factors for the turbulent velocity scale and have found that the results are not sensitive to their detailed form, provided 1) the enhancement factor for K_x is capped at low Langmuir numbers, and 2) the enhancement factors for K_x and V_t are set differently, with higher values for V_t. The latter condition (condition 2) is consistent with the previous scaling suggestions regarding the differences between the near-surface Langmuir mixing and the thermocline entrainment.

While the surface current and temperature are the most important quantities for air–sea interaction affecting tropical cyclone dynamics, the mixing scheme should also provide accurate prediction of the subsurface current and temperature. We find that the mixing layer depth can exceed 200 m on the right side of a slow-moving storm. To examine performance at depth we present a typical example of the vertical profiles of current magnitude and temperature from the one-dimensional model with the various KPP methods and from LES–LT (Fig. 12). The current direction is not greatly impacted by the different parameterizations and is not shown. Here, the results from the tropical cyclone with the moderate ($5\,\mathrm{m\,s^{-1}}$) translation speed and the 10-m initial mixed layer depth are presented, but they are qualitatively similar for all experiments. The KPP–LT results show the best agreement with the LES–LT current profiles (top panels), with some minor discrepancy in the current shear profile near the base of the mixing layer. The KPP–Lag does not correctly predict the mixing in the upper 30 m, although it performs better than the KPP–iLT. For the temperature anomaly profile (where the initial stratification has been subtracted from the simulated temperature profile), the KPP–LT performs slightly better than the other KPP methods, although the differences are small.

We examine the bulk impact of the various KPP mixing schemes by comparing the mixed layer depth h_{ML} from the one-dimensional model and from the LES–LT (Fig. 13). Here, the definition of h_{ML} is the depth where the maximum vertical temperature gradient $\partial\Theta/\partial z$ occurs. These results show that h_{ML} from the
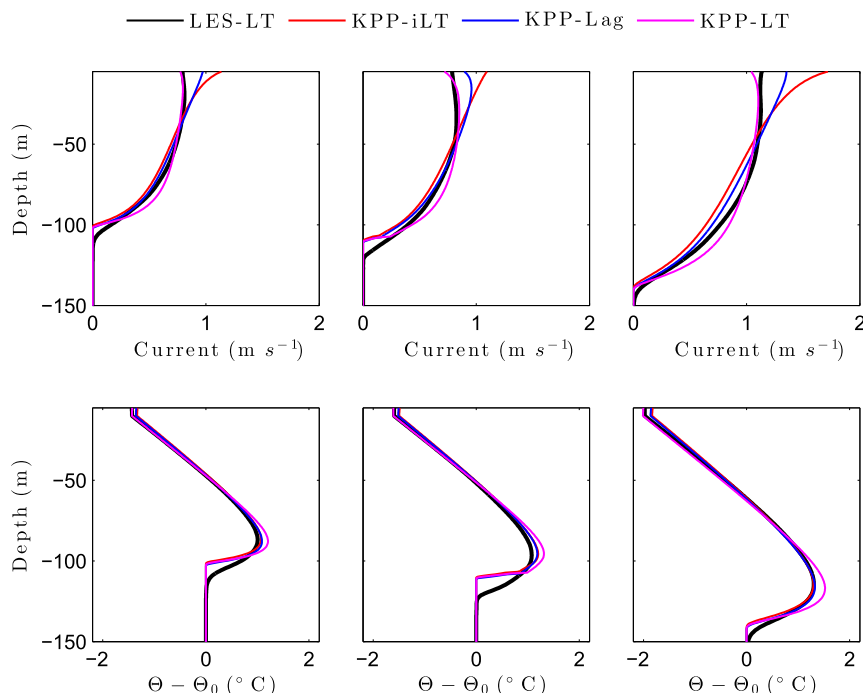
FIG. 12. Vertical profiles (from experiments listed in legend) of (top) current magnitude and (bottom) temperature anomaly (temperature minus initial temperature) at time of peak wind. The test sites are (left) 60 km to the left, (center) the storm center, and (right) 50 km to the right.

KPP–LT agrees best with h_{ML} from the LES–LT compared to KPP–iLT and KPP–Lag (giving the smallest RMS difference). The reason why the LES mixed layer is deeper than the KPP prediction at later times is likely because in the LES there is still some residual turbulence that contributes to mixing near the base of the mixed layer even after the mixing layer depth has shoaled. We have also examined the mixing layer depth h with the different KPP mixing schemes and have found that the results are similar to those of the mixed layer depth h_{ML}.

9. Constant moderate wind experiment

An additional test is performed to assess the performance of the KPP models under a constant moderate wind ($10 \, \mathrm{m \, s^{-1}}$) condition as described in section 3. The results at the end of the experiment are shown in Fig. 14. The right panel shows the temperature anomaly, where the initial temperature profile for the constant wind experiment (defined in section 3) is subtracted from the temperature profile. While the KPP–Lag and KPP–iLT
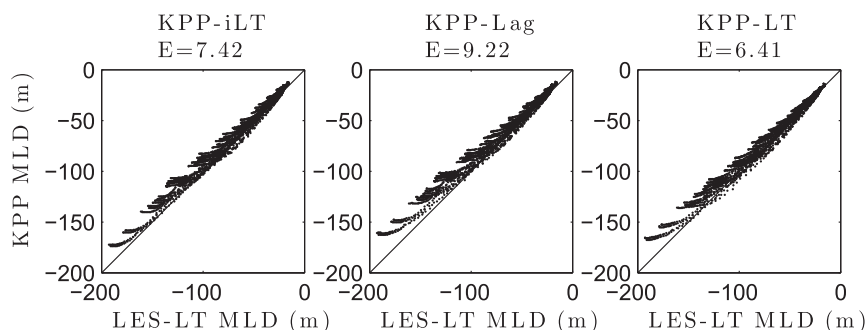
FIG. 13. Mixed layer depth (defined as depth where maximum $\partial\Theta/\partial z$ occurs) from all simulations comparing LES–LT with (left) KPP–iLT, (center) KPP–Lag, and (right) KPP–LT for both translation speeds and both initial mixed layer depths. The value E is the RMS difference computed over all points.
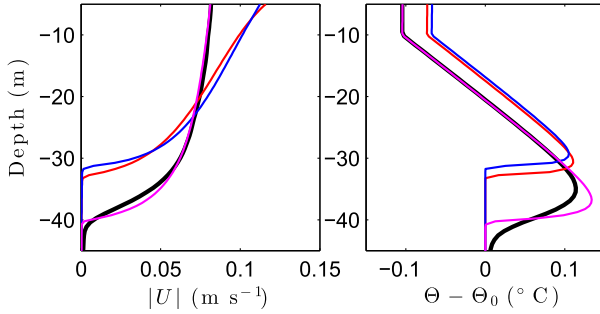
FIG. 14. Vertical profiles at 24 h (left) for current magnitude and (right) for temperature anomaly (temperature minus initial temperature) for a constant $10 \, \text{m s}^{-1}$ experiment. The colors represent the same experiments as in Fig. 12.

models perform similarly in this test, they both underpredict the cooling and deepening of the mixed layer. The KPP–LT results yield the best agreement with the LES model, even if the model tuning has been done in high-wind, tropical cyclone conditions. This experiment suggests that the improved performance of the KPP–LT model is largely due to the enhancement factors (both in the mixing coefficient and V_t) rather than using the Lagrangian shear in place of the Eulerian shear.

Global climate models that use the standard KPP (no Langmuir turbulence) tend to produce positive temperature biases and shallow mixed layer biases in the Southern Ocean compared to observations (see Fan and Griffies 2014). These biases are consistent with the warm temperature bias and underpredicted mixed layer depth produced by KPP–iLT in this constant wind experiment. Fan and Griffies (2014) suggest that Langmuir turbulence may be a missing component of the KPP model in the current global climate models that would lead to underpredicted mixing. The Southern Ocean is where this impact is primarily observed due to the consistent wind forcing and resulting large swells. The best performance of the KPP–LT model in the constant wind experiment suggests that it may be a suitable replacement of KPP–iLT in climate models to reduce biases in these regions.

10. Conclusions

We have developed a series of KPP models and have tested their performance against equivalent LES model simulations in idealized tropical cyclone conditions. The standard KPP model, without the explicit effects of the Langmuir turbulence, does a reasonable job in predicting the mixing layer depth and the surface cooling under an idealized tropical cyclone, but it yields inaccurate prediction of the near-surface turbulent mixing and the

mean current profile. When the KPP is retuned to remove the implicit Langmuir turbulence impact, it adequately reproduces the mean current and temperature simulated by the LES model without the wave effects (shear only mixing).

Replacing the Eulerian currents with the Lagrangian currents in this retuned KPP model improves the currents but degrades the surface cooling compared to the standard KPP model. The turbulent mixing coefficient estimated from the LES results is significantly larger than in the KPP model, that is, the KPP with the Lagrangian currents underpredicts turbulent mixing. The KPP parameterization of the mixing coefficient is improved by introducing an enhancement factor of the turbulent velocity scale, which is dependent on the Langmuir number. Separate enhancement factors are needed for the turbulent mixing coefficient and for the unresolved turbulent shear contribution.

This new modified version of the KPP model, with the Lagrangian currents replacing the Eulerian currents and the enhanced turbulent velocity scales, performs much better than the standard version of the KPP for predicting both temperature and current profiles under a tropical cyclone. This modified KPP model also performs best under constant moderate wind conditions ($10 \, \text{m s}^{-1}$). The improvement compared to the standard KPP model suggests that the new model may reduce undermixing biases that have been previously documented in global climate model simulations in the regions with consistent wind forcing and large swells.

Here, we present the summarized KPP–LT scheme (as implemented in this study). This KPP scheme is used to solve for the vertical turbulent momentum and heat (scalar) fluxes:

$$\overline{\mathbf{u}'_h w'} = -K(\sigma) \frac{\partial \mathbf{U}_{hL}}{\partial z}, \quad \text{and} \tag{35}$$

$$\overline{\theta' w'} = -K(\sigma) \frac{\partial \Theta}{\partial z}. \tag{36}$$

The mixing coefficient is set as

$$K(\sigma) = hWG(\sigma)F_{\text{LT}}^K(\sigma), \tag{37}$$

where h is determined as the shallowest depth at which the bulk Richardson number

$$\text{Ri}_b(z) = \frac{[B^r - B(z)]|z|}{[U_L^r - U_L(z)]^2 + [V_L^r - V_L(z)]^2 + [V_t(z)F_{\text{LT}}^{V_t}]^2} \tag{38}$$

exceeds the critical value (0.235 for this study). The enhancement of the unresolved turbulence is set as

$$F_{LT}^{Vt} = 1 + 2.3 La_{SL\theta'}^{-1/2}, \qquad (39)$$

and the enhancement to the turbulent mixing coefficient is set as

$$F_{LT}^{K}(\sigma) = 1 + (F_{LT}' - 1)G(\sigma)/\max[G(\sigma)], \qquad (40)$$

$$F_{LT}' = 1 + La_{SL\theta'}^{-1}, \quad La_{SL\theta'} \geq 0.8, \quad \text{and} \qquad (41)$$

$$F_{LT}' = 2.25, \quad La_{SL\theta'} \leq 0.8. \qquad (42)$$

The next step of this research will be to introduce this modified KPP model into three-dimensional ocean models. This will allow the impact of the Langmuir turbulence to be more thoroughly evaluated against available in situ observations.

REFERENCES

Craig, P. D., and M. L. Banner, 1994: Modeling wave-enhanced turbulence in the ocean surface layer. *J. Phys. Oceanogr.*, **24**, 2546–2559, doi:10.1175/1520-0485(1994)024<2546:MWETIT>2.0.CO;2.

Craik, A. D. D., and S. Leibovich, 1976: A rational model for Langmuir circulations. *J. Fluid Mech.*, **73**, 401–426, doi:10.1017/S0022112076001420.

D'Alessio, J. S. D., K. Abdella, and N. A. McFarlane, 1998: A new second-order turbulence closure scheme for the oceanic mixed layer. *J. Phys. Oceanogr.*, **28**, 1624–1641, doi:10.1175/1520-0485(1998)028<1624:ANSOTC>2.0.CO;2.

D'Asaro, E., J. Thomson, A. Shcherbina, R. Harcourt, M. Cronin, M. Hemer, and B. Fox-Kemper, 2014: Quantifying upper ocean turbulence driven by surface waves. *Geophys. Res. Lett.*, **41**, 102–107, doi:10.1002/2013GL058193.

Emanuel, K. A., 1991: The theory of hurricanes. *Annu. Rev. Fluid Mech.*, **23**, 179–196, doi:10.1146/annurev.fl.23.010191.001143.

——, 1999: Thermodynamic control of hurricane intensity. *Nature*, **401**, 665–669, doi:10.1038/44326.

Fan, Y., and S. M. Griffies, 2014: Impacts of parameterized Langmuir turbulence and nonbreaking wave mixing in global climate simulations. *J. Climate*, **27**, 4752–4775, doi:10.1175/JCLI-D-13-00583.1.

——, I. Ginis, T. Hara, C. W. Wright, and E. J. Walsh, 2009: Numerical simulations and observations of surface wave fields under an extreme tropical cyclone. *J. Phys. Oceanogr.*, **39**, 2097–2116, doi:10.1175/2009JPO4224.1.

Ginis, I., 2002: Tropical cyclone–ocean interactions. *Atmosphere–Ocean Interactions, Volume 1*, W. Perrie, Ed., Advances in Fluid Mechanics Series, No. 22, WIT Press, 83–114.

Grant, A. L. M., and S. E. Belcher, 2009: Characteristics of Langmuir turbulence in the ocean mixed layer. *J. Phys. Oceanogr.*, **39**, 1871–1887, doi:10.1175/2009JPO4119.1.

Griffies, S. M., M. Levy, A. J. Adcroft, G. Danabasoglu, D. Jacobsen, W. Large, and T. Ringler, 2013: Theory and numerics of the Community Ocean Vertical Mixing (CVMIX) project. Tech. Rep., 94 pp. [Available online at https://cvmix.googlecode.com/svn/trunk/manual/cvmix.pdf.]

Harcourt, R. R., 2013: A second-moment closure model of Langmuir turbulence. *J. Phys. Oceanogr.*, **43**, 673–697, doi:10.1175/JPO-D-12-0105.1.

——, 2015: An improved second-moment closure model of Langmuir turbulence. *J. Phys. Oceanogr.*, **45**, 84–103, doi:10.1175/JPO-D-14-0046.1.

——, and E. A. D'Asaro, 2008: Large-eddy simulation of Langmuir turbulence in pure wind seas. *J. Phys. Oceanogr.*, **38**, 1542–1562, doi:10.1175/2007JPO3842.1.

Holland, G. J., 1980: An analytic model of the wind and pressure profiles in hurricanes. *Mon. Wea. Rev.*, **108**, 1212–1218, doi:10.1175/1520-0493(1980)108<1212:AAMOTW>2.0.CO;2.

Hong, S.-Y., and H.-L. Pan, 1996: Nonlocal boundary layer vertical diffusion in a medium-range forecast model. *Mon. Wea. Rev.*, **124**, 2322–2339, doi:10.1175/1520-0493(1996)124<2322:NBLVDI>2.0.CO;2.

Kantha, L. H., and C. A. Clayson, 2004: On the effect of surface gravity waves on mixing in the oceanic mixed layer. *Ocean Modell.*, **6**, 101–124, doi:10.1016/S1463-5003(02)00062-8.

Kukulka, T., A. J. Plueddemann, J. H. Trowbridge, and P. P. Sullivan, 2009: Significance of Langmuir circulation in upper ocean mixing: Comparison of observations and simulations. *Geophys. Res. Lett.*, **36**, L10603, doi:10.1029/2009GL037620.

——, ——, ——, and ——, 2010: Rapid mixed layer deepening by the combination of Langmuir and shear instabilities: A case study. *J. Phys. Oceanogr.*, **40**, 2381–2400, doi:10.1175/2010JPO4403.1.

Langmuir, I., 1938: Surface motion of water induced by wind. *Science*, **87**, 119–123, doi:10.1126/science.87.2250.119.

Large, W. G., J. C. McWilliams, and S. C. Doney, 1994: Oceanic vertical mixing: A review and a model with a nonlocal boundary layer parameterization. *Rev. Geophys.*, **32**, 363–403, doi:10.1029/94RG01872.

McWilliams, J. C., and J. M. Restrepo, 1999: The wave-driven ocean circulation. *J. Phys. Oceanogr.*, **29**, 2523–2540, doi:10.1175/1520-0485(1999)029<2523:TWDOC>2.0.CO;2.

——, and P. P. Sullivan, 2000: Vertical mixing by Langmuir circulations. *Spill Sci. Technol. Bull.*, **6**, 225–237, doi:10.1016/S1353-2561(01)00041-X.

——, ——, and C.-H. Moeng, 1997: Langmuir turbulence in the ocean. *J. Fluid Mech.*, **334**, 1–30, doi:10.1017/S0022112096004375.

——, E. Huckle, J.-H. Liang, and P. P. Sullivan, 2012: The wavy Ekman layer: Langmuir circulations, breaking waves, and Reynolds stress. *J. Phys. Oceanogr.*, **42**, 1793–1816, doi:10.1175/JPO-D-12-07.1.

——, ——, ——, and ——, 2014: Langmuir turbulence in swell. *J. Phys. Oceanogr.*, **44**, 870–890, doi:10.1175/JPO-D-13-0122.1.

Mellor, G. L., and T. Yamada, 1982: Development of a turbulence closure model for geophysical fluid problems. *Rev. Geophys. Space Phys.*, **20**, 851–875, doi:10.1029/RG020i004p00851.

Melville, W. K., 1996: The role of surface-wave breaking in air-sea interaction. *Annu. Rev. Fluid Mech.*, **28**, 279–321, doi:10.1146/annurev.fl.28.010196.001431.

Min, H. S., and Y. Noh, 2004: Influence of the surface heating on Langmuir circulation. *J. Phys. Oceanogr.*, **34**, 2630–2641, doi:10.1175/JPOJPO-2654.1.

Moon, I.-J., I. Ginis, T. Hara, H. L. Tolman, C. W. Wright, and E. J. Walsh, 2003: Numerical simulation of sea surface directional wave spectra under hurricane wind forcing. *J. Phys. Oceanogr.*, **33**, 1680–1706, doi:10.1175/2410.1.

Noh, Y., H. S. Min, and S. Raasch, 2004: Large eddy simulation of the ocean mixed layer: The effects of wave breaking and Langmuir circulation. *J. Phys. Oceanogr.*, **34**, 720–735, doi:10.1175/1520-0485(2004)034<0720:LESOTO>2.0.CO;2.

——, G. Goh, and S. Raasch, 2011: Influence of Langmuir circulation on the deepening of the wind-mixed layer. *J. Phys. Oceanogr.*, **41**, 472–484, doi:10.1175/2010JPO4494.1.

Polton, J. A., and S. E. Belcher, 2007: Langmuir turbulence and deeply penetrating jets in an unstratified mixed layer. *J. Geophys. Res.*, **112**, C09020, doi:10.1029/2007JC004205.

Price, J. F., 1981: Upper ocean response to a hurricane. *J. Phys. Oceanogr.*, **11**, 153–175, doi:10.1175/1520-0485(1981)011<0153:UORTAH>2.0.CO;2.

Rabe, T. J., T. Kukulka, I. Ginis, T. Hara, B. G. Reichl, E. A. D'Asaro, R. R. Harcourt, and P. P. Sullivan, 2015: Langmuir turbulence under Hurricane Gustav (2008). *J. Phys. Oceanogr.*, **45**, 657–677, doi:10.1175/JPO-D-14-0030.1.

Sanford, T. B., J. F. Price, and J. B. Girton, 2011: Upper-ocean response to Hurricane Frances (2004) observed by profiling EM-APEX floats. *J. Phys. Oceanogr.*, **41**, 1041–1056, doi:10.1175/2010JPO4313.1.

Sinha, N., A. E. Tejada-Martinez, C. Akan, and C. E. Grosch, 2015: Toward a K-profile parameterization of Langmuir turbulence in shallow coastal shelves. *J. Phys. Oceanography*, **45**, 2869–2895, doi:10.1175/JPO-D-14-0158.1.

Skyllingstad, E. D., and D. W. Denbo, 1995: An ocean large-eddy simulation of Langmuir circulations and convection in the surface mixed layer. *J. Geophys. Res.*, **100**, 8501–8522, doi:10.1029/94JC03202.

——, W. D. Smyth, and G. B. Crawford, 2000: Resonant wind-driven mixing in the ocean boundary layer. *J. Phys. Oceanogr.*, **30**, 1866–1890, doi:10.1175/1520-0485(2000)030<1866:RWDMIT>2.0.CO;2.

Smyth, W. D., E. D. Skyllingstad, G. B. Crawford, and H. Wijesekera, 2002: Nonlocal fluxes and Stokes drift effects in the K-profile parameterization. *Ocean Dyn.*, **52**, 104–115, doi:10.1007/s10236-002-0012-9.

Sullivan, P. P., J. C. McWilliams, and W. K. Melville, 2007: Surface gravity wave effects in the oceanic boundary layer: Large-eddy simulation with vortex force and stochastic breakers. *J. Fluid Mech.*, **593**, 405–452, doi:10.1017/S002211200700897X.

——, L. Romero, J. C. McWilliams, and W. K. Melville, 2012: Transient evolution of Langmuir turbulence in ocean boundary layers driven by hurricane winds and waves. *J. Phys. Oceanogr.*, **42**, 1959–1980, doi:10.1175/JPO-D-12-025.1.

Teixeira, M. A. C., and S. E. Belcher, 2010: On the structure of Langmuir turbulence. *Ocean Modell.*, **31**, 105–119, doi:10.1016/j.ocemod.2009.10.007.

Terray, E. A., M. A. Donelan, Y. C. Agrawal, W. M. Drennan, K. K. Kahma, A. J. Williams III, P. A. Hwang, and S. A. Kitaigorodskii, 1996: Estimates of kinetic energy dissipation under breaking waves. *J. Phys. Oceanogr.*, **26**, 792–807, doi:10.1175/1520-0485(1996)026<0792:EOKEDU>2.0.CO;2.

Tolman, H. L., 2009: User manual and system documentation of WAVEWATCH III version 3.14. NOAA/NWS/NCEP/EMC/MMAB Tech. Note 276, 220 pp.

Umlauf, L., H. Burchard, and K. Bolding, 2005: GOTM: Scientific documentation. 3rd ed. Leiniz-Institute for Baltic Sea Research Marine Science, 360 pp. [Available online at http://www.gotm.net/pages/documentation/manual/stable/pdf/a4.pdf.]

Van Roekel, L. P., B. Fox-Kemper, P. P. Sullivan, P. E. Hamlington, and S. R. Haney, 2012: The form and orientation of Langmuir cells for misalinged winds and waves. *J. Geophys. Res.*, **117**, C05001, doi:10.1029/2011JC007516.

Yablonsky, R. M., and I. Ginis, 2009: Limitation of one-dimensional ocean models for coupled hurricane–ocean model forecasts. *Mon. Wea. Rev.*, **137**, 4410–4419, doi:10.1175/2009MWR2863.1.

Young, I. R., 2003: A review of the sea state generated by hurricanes. *Mar. Struct.*, **16**, 201–218, doi:10.1016/S0951-8339(02)00054-0.

Zhang, J. A., and E. W. Uhlhorn, 2012: Hurricane sea surface inflow angle and an observation-based parametric model. *Mon. Wea. Rev.*, **140**, 3587–3605, doi:10.1175/MWR-D-11-00339.1.